Tumor tissues were harvested after sacrifice of the mice and the lysates were prepared as described (10).

Construction of a Skp2 expression plasmid

Skp2 cDNA was amplified to construct a Skp2 expression plasmid with RT-PCR using a pair of oligonucleotide primers specific to the coding sequence of human Skp2 (forward 5′-ACACAAGCTTATGGATTACAAGGATGACGACGATAAGATGCACAGGAAGCACCTC-3′, including a Flag tag sequence, and reverse 5′-ACACCTCGAGTCATAGACAACTGGGCTTTTGCAGTGTCAG-3′). PCR amplification for constructing an expression plasmid for Skp2-LRR was done using another forward primer (5′-ACC AAGCTTATGGATTACAAGGATGACGACGATAAGTTAGACCTCACAGGTAA-3′, including a Flag tag) and the reverse primer for human Skp2 described above. The PCR products were inserted into pcDNA3.1.

Secreted placental alkaline phosphatase (SEAP) reporter assay

A reporter construct, pMyc-SEAP (Clontech Laboratories, Inc), which contains several E-boxes at the 5′ of the TATA-like promoter, was used to measure Myc activity, and a control construct containing only the basic TATA like promoter, pTAL-SEAP, was used as a negative control to measure activity of the basal TATA-like promoter. pMyc-SEAP or pTAL-SEAP was transfected into HepG2 cells with other expression plasmids. After 24 hours, the medium was replaced with fresh medium with or without HGF (50 ng/mL) in the absence or presence of PD98059. The cells were cultured for another 24 hours, and the medium was used for SEAP assays (Clontech Laboratories, Inc). To determine the net activity of SEAP, the activity in cells with the negative control (pTAL-SEAP) was used as a background value. All values were normalized with activity of β-gal, which was cotransfected with the reporter.

Silencing by siRNA

Synthetic siRNAs for Id1, Myc, and Skp2 were obtained from Integrated DNA Technologies, Inc. Detailed methods were described in Supplementary Data.

Luciferase reporter assays

The p16 promoter construct containing −247 to +1 from the transcription initiation site of the *p16* gene (kindly provided by Dr. E. Hara, Japan Foundation for Cancer Research, and described previously in ref. 9) was cotransfected with an expression plasmid for Skp2 and a standard amount of the pSV-β-galactosidase control plasmid (Promega). HGF treatment of the cells and luciferase reporter assays were conducted as previously described (9, 10).

Image manipulation

Adjustments of brightness and contrast with a linear algorithm were applied to the whole image.

Statistical analysis

The paired Student *t* test was used to test for significance where indicated.

Results

HGF downregulates Skp2 expression at the mRNA and protein level in an ERK-dependent manner

We found that injection of HGF into established tumors originating from HepG2 cells in NOD/SCID mice significantly downregulated Skp2 (Fig. 1A). Skp2 has transformation activity in experimental models, and is sometimes overexpressed in human cancers. To determine the role and mechanism of the downregulation of Skp2, we first conducted a time-course analysis of Skp2 expression in HepG2 cells treated with HGF. Western blot analysis showed that the level decreased for 24 hours, and remained low after 24 hours (Fig. 1B). As HGF treatment suppresses the proliferation of HepG2 cells through strong ERK activity (7, 9, 25), we examined the effect of ERK activity on the expression of Skp2. Treatment with a low concentration of PD98059, which partially inhibits ERK activity and restores cell proliferation suppressed by HGF (7, 9), restored the amount of Skp2 protein (Fig. 1B), indicating that Skp2 expression is regulated in an ERK-dependent manner, and suggesting the relevance of Skp2 to the regulation of cell proliferation. RT-PCR analysis showed that Skp2 mRNA expression was also downregulated by HGF and the amount of Skp2 mRNA was restored by a low concentration of PD98059 (Fig. 1C), showing that Skp2 expression is regulated at the transcription level in an ERK-dependent manner. HGF treatment of another hepatoma cell line, HuH7, proliferation of which is suppressed by HGF in an ERK-dependent manner (Supplementary Fig. S1), also led to ERK-dependent downregulation of Skp2 mRNA (Fig. 1D), suggesting that cancer cells other than HepG2 cells also are responsive to HGF.

To confirm that the strong ERK activity mediates the Skp2 downregulation, we used a HepG2 cell line, in which ERK activity is strongly activated by induction of active Ras (Ras V12) with Isopropyl-β-D(−)-thiogalactopyranoside (IPTG; ref. 7). Induction of the Ras, which suppressed proliferation of HepG2 cells, downregulated Skp2 (Fig. 1E), indicating that strong ERK activation is sufficient for downregulation of Skp2, and supporting that the expression of Skp2 is related to the regulation of proliferation in HepG2 cells.

Downregulation of Skp2 is not involved in the upregulation of p27, while it is involved in the suppression of cell proliferation with HGF

Figure 1B (left) shows that the timing of Skp2 downregulation after HGF treatment coincided with that of p27 upregulation. The expression of p27 mRNA was not altered by HGF (Supplementary Fig. S2), consistent with a report that p27 expression is regulated at the level of protein degradation via Skp2 (26). However, the partial inhibition of ERK activity with the low concentration of PD98059 had no effect on the upregulation of p27 by HGF, and p27 protein expression remained upregulated, even though the level of Skp2 protein was high (Fig. 1B, right). Moreover, with the HepG2 cell line, in which ERK is strongly activated by induction of active Ras with IPTG, we showed that activation of Ras did not alter the level of p27, while it

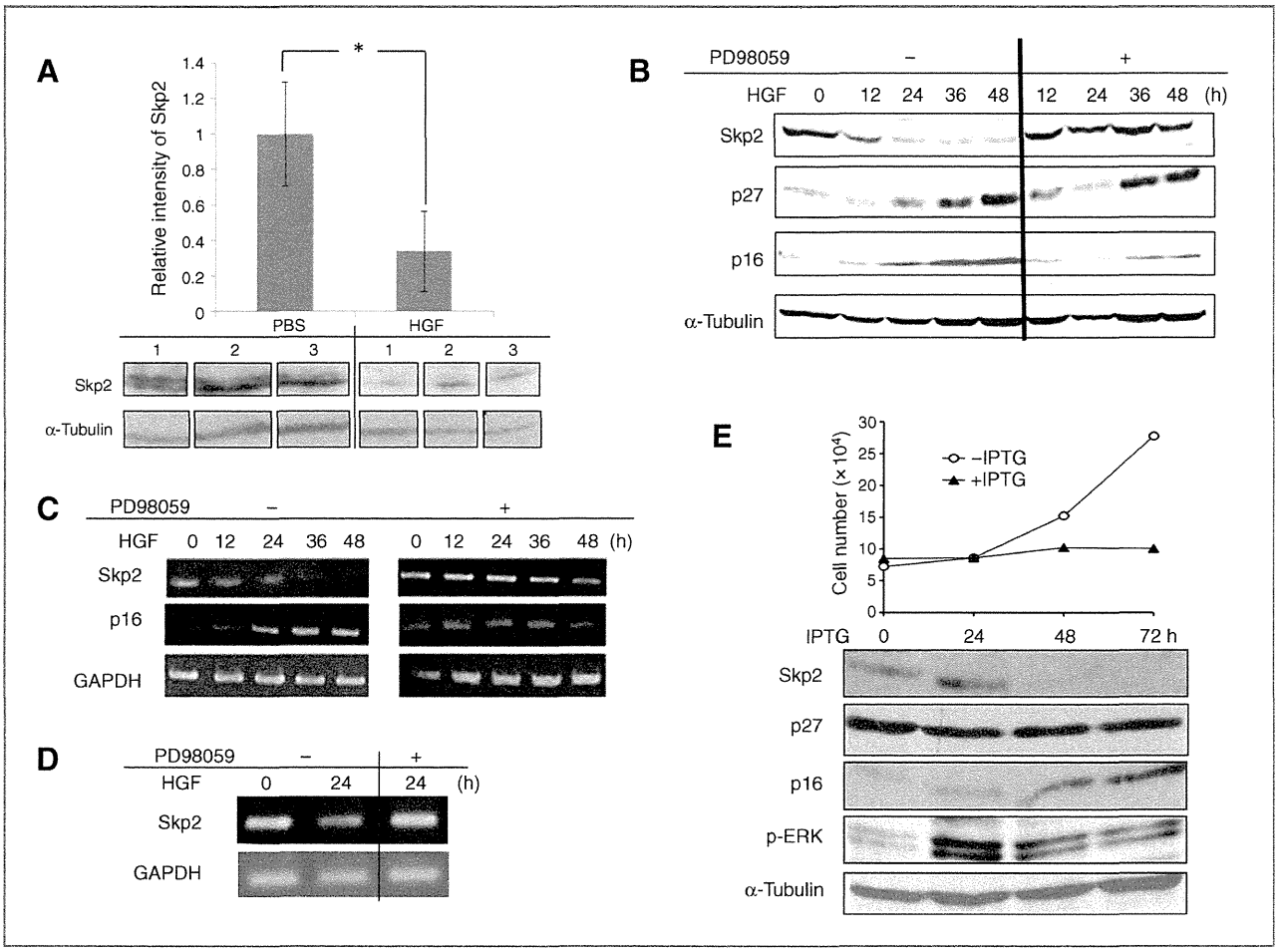

Figure 1. Skp2 is downregulated by HGF in an ERK-dependent manner. A, Western blot analysis to detect Skp2 in established tumors from HepG2 cells in NOD/SCID mice. All bands in analysis with anti-Skp2 and α-tubulin antibodies, respectively, were acquired from a single film exposure. Unprocessed full-length blots are presented in Supplementary Fig. S4. The intensity of the band in the bottom was quantitated using NIH ImageJ software and graphed. Each value represents the mean ± S.D. ($n = 3$). *, $P < 0.05$; Student t test. B, Western blot analysis to detect Skp2 and p27 in HepG2 cells treated with HGF in the absence (–) or presence (+) of PD98059. Cell lysates were prepared at the indicated times (h) after HGF treatment and subjected to Western blot analysis. Tubulin was used as a loading control. p16 is shown to assess the effect of HGF. The result is representative of three independent experiments. C, RT-PCR analysis of Skp2 in HepG2 cells treated with HGF in the absence (–) or presence (+) of PD98059. Total RNA was purified at the indicated times and subjected to RT-PCR. GAPDH was used as an internal control. p16 is shown to assess the effect of HGF. The result is representative of two independent experiments. D, RT-PCR analysis of Skp2 in HuH7 cells treated with or without HGF for 24 hours in the absence (–) or presence (+) of PD98059. Total RNA was purified and subjected to RT-PCR. GAPDH was used as an internal control. E, time course analysis of cell proliferation (top) and Western blot analysis to detect Skp2 and p27 in cells with forced activation of ERK (bottom). After the active form of Ras was induced with IPTG, cell numbers were counted and cell lysates were prepared at the indicated times after induction. Phospho-ERK and p16 are shown to assess the effect of Ras induction. Experiments were done twice with similar results, and representative data are shown.

downregulated Skp2 expression (Fig. 1E). These results suggested that the downregulation of Skp2 is not involved in the upregulation of p27. They also showed that the upregulation of p27 by HGF is not mediated by the ERK activity, and suggested that the upregulation is not involved in the inhibitory effect of HGF on HepG2 cell proliferation.

To directly show that the downregulation of Skp2 is not involved in the upregulation of p27, experiments with high expression of Skp2 were conducted. HepG2 cells were transfected with Skp2, and the protein levels of Skp2 and p27 were examined by Western blot analysis after HGF treatment. High expression of Skp2 did not suppress the upregulation of p27 (Fig. 2A), showing the upregulation to be independent of the downregulation of Skp2. In contrast, cell counts showed that high expression of Skp2 restored the cell proliferation suppressed by HGF (Fig. 2B), indicating that downregulation of Skp2 is essential for the inhibitory effect of HGF on the proliferation of the cells. The data also suggested that the upregulation of p27 is not involved in the inhibitory effect of HGF, as high expression of Skp2 did not suppress the upregulation (Fig. 2A). Although the number of cells was restored with high expression of Skp2 in the presence of HGF, it did not reach the number achieved in the absence of HGF (Fig. 2B). This may simply be due to the transfection efficiency of the construct to express Skp2.

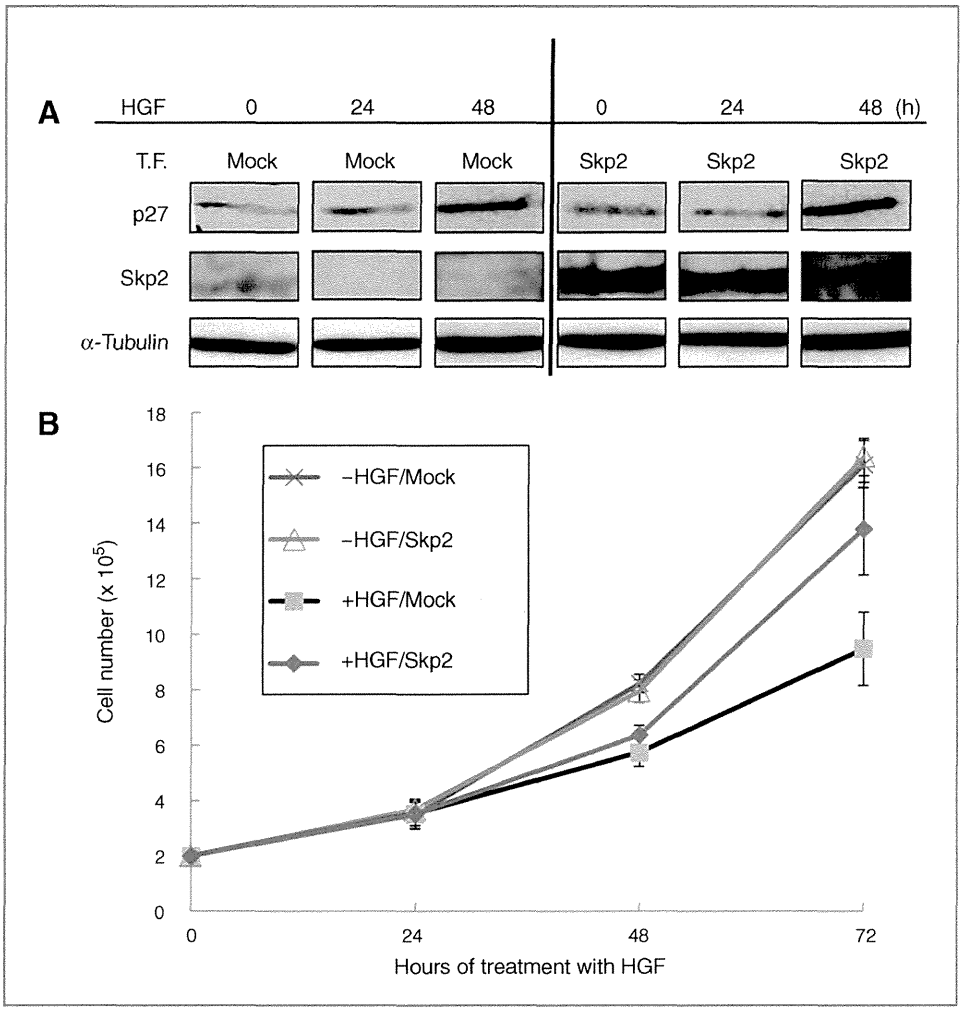

Figure 2. High expression of Skp2 has no effect on p27, but restores cell proliferation suppressed with HGF. A, Western blot analysis to detect p27 in cells with high expression of Skp2. All bands in analysis with anti-p27, Skp2, and α-tubulin antibodies, respectively, were acquired from a single film exposure. Full-length blots are presented in Supplementary Fig. S5. B, time course analysis of proliferation in cells transfected with Skp2 in the absence or presence of HGF. Cells were prepared as described in (A) and cell numbers were counted at the indicated times. Each value represents the mean ± S.D. of triplicate determinants. The results are representative of three independent experiments.

Downregulation of Skp2 with HGF reduces Myc activity

A few reports have indicated that Skp2 has another role in activation of the transcription factor Myc (18, 19), and Myc was reported to have important roles in hepatocarcinoma (21, 22). A recent report showed that knockdown of Myc suppressed proliferation of HepG2 cells (27), and we obtained results consistent with this by knockdown of Myc (data not shown), indicating that Myc expression is required for the proliferation of HepG2 cells. Thus, we studied the relevance of Skp2 to Myc in HepG2 hepatoma cells. We first examined Myc activity in HepG2 cells treated with HGF. A promoter-reporter construct, in which the SEAP reporter gene is regulated by binding of Myc on the promoter, was introduced into the cells, and the SEAP activity was analyzed in the absence or presence of HGF with or without the low concentration of PD98059. HGF treatment of the cells greatly reduced endogenous Myc activity, and the partial inhibition of ERK activity with PD98059 significantly restored the Myc activity suppressed by HGF (Fig. 3A), indicating that the Myc activity is regulated by HGF in an ERK-dependent manner. To know which Myc family proteins are involved in the Myc activity in HepG2 cells, we examined the levels of c-myc, N-myc, and L-myc by RT-PCR. The expression of c-myc was much higher than that of the others (data not shown). Thus, the Myc activity seems to be mostly derived from c-Myc in the cells.

As the Myc protein is known to be unstable (28), it is possible that the inactivation of Myc with HGF simply reflects loss of the protein. However, Western blot analysis showed that the amount of c-Myc is not altered in the presence of HGF (Fig. 3B), suggesting that the reduction in Myc activity with HGF is not caused by loss of the protein. We also analyzed the levels of Max and Mad, because in the Myc/Max/Mad network, the association of Myc with Max leads to transcriptional activation, and that of Mad with Max to repression (29). We did not detect any changes in their expressions in HepG2 cells treated with HGF (Supplementary Fig. S3), suggesting that the reduction in Myc activity by HGF is not regulated by changes in the amounts of Mad and Max.

As the reduction in Myc activity by HGF is mediated through the strong ERK activity, it may be caused by the downregulation of Skp2. We thus examined whether Skp2 regulates endogenous Myc activity. We introduced the

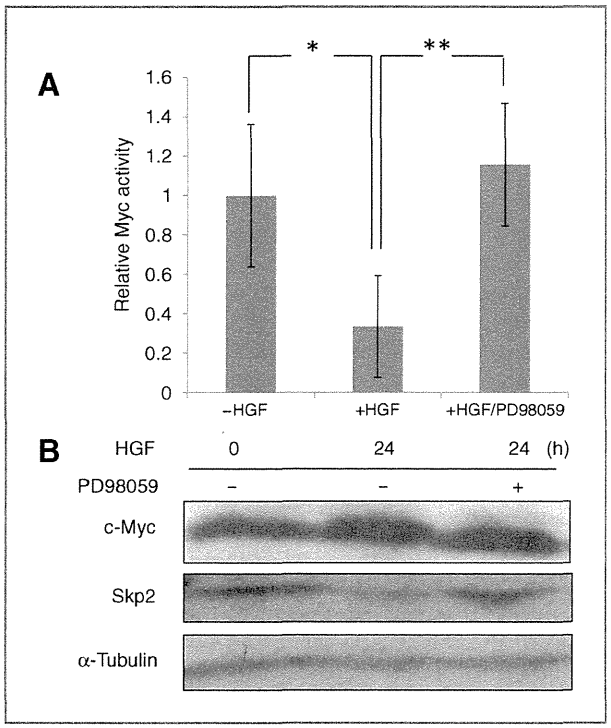

Figure 3. HGF treatment reduces Myc activity, but does not alter the amount of c-Myc. A, detection of endogenous Myc activity in cells treated with HGF in the absence or presence of PD98059. All values were normalized as described in Materials and Methods. The average fold-increase in Myc activity compared with activity in the absence of HGF without PD98059 is indicated. Each value represents the mean ± S.D. of triplicate determinants from a representative experiment. *, $P < 0.05$; **, $P < 0.01$, Student t test. B, Western blot analysis to detect c-Myc. Cells were treated with HGF in the absence or presence of PD98059 and cell lysates were prepared at 0 or 24 hours. Skp2 is shown to assess the effect of HGF or HGF plus PD98059. Experiments were carried out twice with similar results, and representative data are shown.

reporter for Myc together with the construct to express Skp2 into the cells. High expression of Skp2 activated Myc activity in the absence or presence of HGF (Fig. 4A), indicating that Skp2 is sufficient to activate endogenous Myc. Next, to directly show that the reduction in Myc activity is caused by the downregulation of Skp2, we introduced Skp2 siRNA into the cells. Knockdown of Skp2 significantly decreased endogenous Myc activity without altering the amount of c-Myc in the absence of HGF (Fig. 4B and C), indicating that Skp2 is essential to activate Myc in proliferating cells. These results showed that Skp2 functions to activate Myc, and thus, downregulation of Skp2 results in the reduction in Myc activity.

Myc activity is regulated by Skp2, but not through SCF^{Skp2}

It was previously shown that Myc is activated via ubiquitination by the SCF complex including Skp2 (SCF^{Skp2}). The ubiquitination results in rapid degradation of Myc (18, 19). However, inhibition of ubiquitination and degradation with knockdown of Skp2 induced no accumulation of Myc

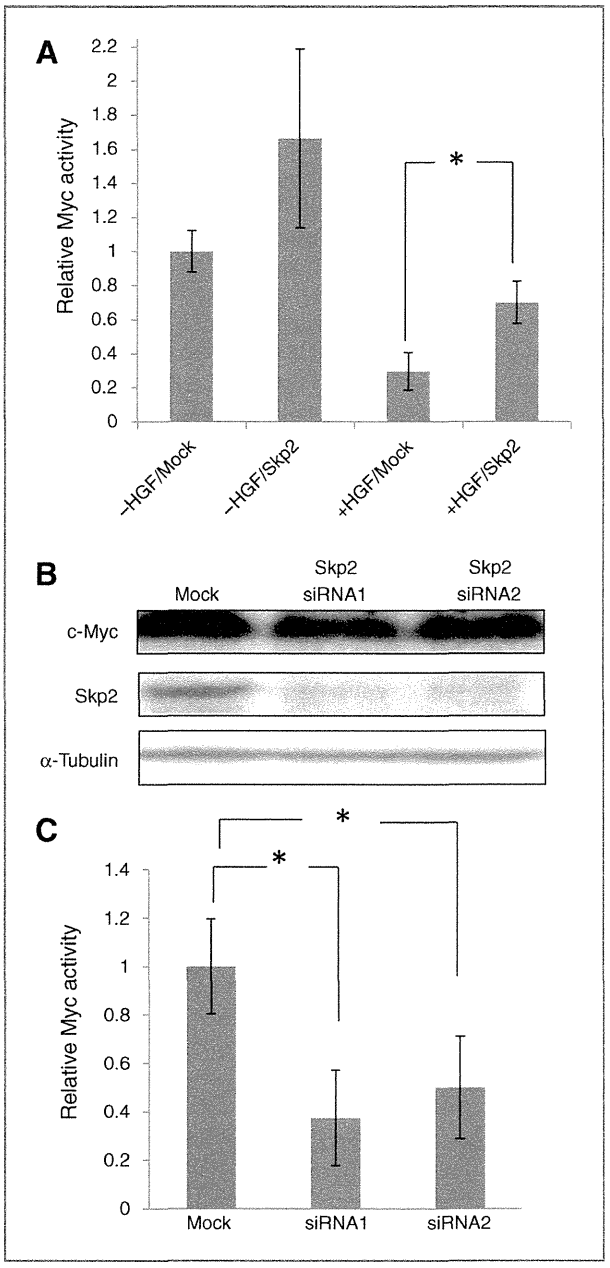

Figure 4. Skp2 is involved in regulation of endogenous Myc activity. A, detection of endogenous Myc activity in cells with high expression of Skp2. The average fold-increase in SEAP activity compared with activity in the absence of HGF with a Mock-transfection is indicated. Each value represents the mean ± S.D. of triplicate determinants from a representative experiment. *, $P < 0.01$; Student t test. B, Western blot analysis to detect c-Myc in cells with Skp2 knockdown. Cells were transfected with two kinds of siRNA targeting Skp2 or randomized siRNA (Mock) as a control. Cell lysates were prepared at 24 hours after transfection and subjected to immunoblotting. Experiments were carried out twice with similar results and representative data are shown. C, detection of endogenous Myc activity in cells with Skp2 knockdown. The average fold-decrease in Myc activity compared with a Mock transfection is indicated. Each value represents the mean ± S.D. of triplicate determinants from a representative experiment. *, $P < 0.001$; Student t test.

protein (Fig. 4B), suggesting that ubiquitination of Myc by SCF^{Skp2} is not involved in the regulation of Myc activity. To directly show whether or not the SCF complex is required for the transcriptional activation of Myc by Skp2, we adopted a mutant of Skp2, Skp2-leucine–rich repeats (LRR), which has a deletion in the N-terminus including a part of the F-box domain, resulting in an inability to couple to the SCF complex (18). High expression of not only the wild-type Skp2 but also Skp2-LRR restored the Myc activity reduced by HGF treatment (Fig. 5A), indicating that Skp2 regulates Myc activity, but ubiquitination of Myc by the SCF complex is not involved in the regulation of Myc activity by Skp2. This idea was supported by the finding that high expression of Skp2 and Skp2-LRR did not change the amount of Myc protein (Fig. 5B).

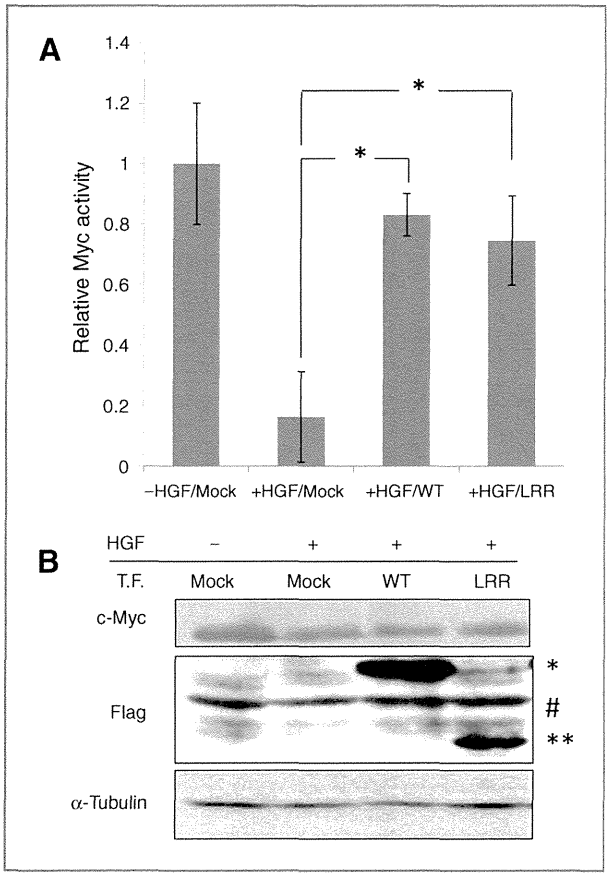

Figure 5. High expression of Skp2-LRR restores Myc activity suppressed by HGF. A, detection of endogenous Myc activity in cells with high expression of Skp2 (WT) or Skp2-LRR (LRR). The average fold-decrease in Myc activity compared with activity in the absence of HGF with a Mock transfection is indicated. Each value represents the mean ± S.D. of triplicate determinants from a representative experiment. *, $P < 0.01$; Student *t* test. B, Western blot analysis to detect c-Myc in cells transfected with Skp2 (WT) or Skp2-LRR (LRR). Exogenous Skp2 and Sk2-LRR were detected with anti-Flag and their positions are indicated with * and **, respectively. The signal represented by # is nonspecific. Experiments were carried out twice with similar results and representative data are shown.

Skp2 is involved in Id1 expression through regulation of Myc activity

Myc regulates transcription of a wide range of genes responsible for regulation of cell proliferation, transcription, cell motility and so on (29). To uncover the target of Myc activated by Skp2 in the hepatoma cells, and to address the mechanism by which Skp2 affects proliferation through HGF signaling, we focused on a transcriptional regulator, Id1: Id1 seemed to be a target of Myc activated by Skp2, because our previous study showed that Id1, whose the mRNA and protein are downregulated by HGF, is involved in the anti-proliferative effect of HGF through regulation of p16 expression (10), and it was recently reported that c-Myc upregulated Id1 expression in human breast cancer cells and prostate cancer cells (30, 31). In addition, Id1 expression in another hepatoma cell line, HuH7, proliferation of which is suppressed by HGF in an ERK-dependent manner (Supplementary Fig. S1), was also regulated in an ERK-dependent manner (Supplementary Fig. S6), suggesting that Id1 is involved in the inhibitory effect of HGF on proliferation of cancer cells other than HepG2. Western blot analysis showed that high expression of Skp2 restored the expression of Id1 suppressed by HGF (Fig. 6A), and knockdown of Skp2 suppressed the expression of Id1 in the absence of HGF (Fig. 6B and Supplementary Fig. S7), showing that Skp2 is involved in the regulation of Id1 expression. In addition, knockdown of Myc suppressed the expression of Id1 in the absence of HGF (Fig. 6C), indicating that Myc regulates Id expression. These results, together with the fact that Skp2 regulates Myc activity, suggest that Skp2 regulates Id1 expression through the regulation of Myc activity. Also, high expression of the Skp2 mutant, Skp2-LRR, restored Id1 expression and cell proliferation suppressed by HGF (Supplementary Fig. S8), suggesting that Id1 expression is regulated by Skp2 in the SCF complex-independent manner. As we previously showed that the downregulation of Id1 results in the activation of the promoter of the *p16* gene (10), we next examined the effect of Skp2 on the promoter. A promoter-reporter construct, in which expression of luciferase is regulated by a minimal promoter of the *p16* gene (9), was introduced into HepG2 cells together with the construct to express Skp2 in the absence or presence of HGF. While HGF treatment of the cells activated the p16 promoter as previously reported (9), high expression of Skp2 significantly suppressed the activation of the p16 promoter (Fig. 6D). Also, knockdown of Id1 restored the promoter activity suppressed by high expression of Skp2 in the presence of HGF (Fig. 6E, lane 3, 4, and 8). These results supported that Skp2 regulates Id1 expression, leading to regulation of p16 promoter. Higher activity of p16 promoter induced by Id1 siRNA (lane 7 and 8) than that induced by randomized siRNA (lane 3 and 4) in the presence of HGF seems to represent a partial reduction, but not complete elimination, of Id1 by HGF treatment of the cells.

Discussion

Recent clinical research suggests that Skp2 has a p27-independent role in some cancer cells (17). In this study, we

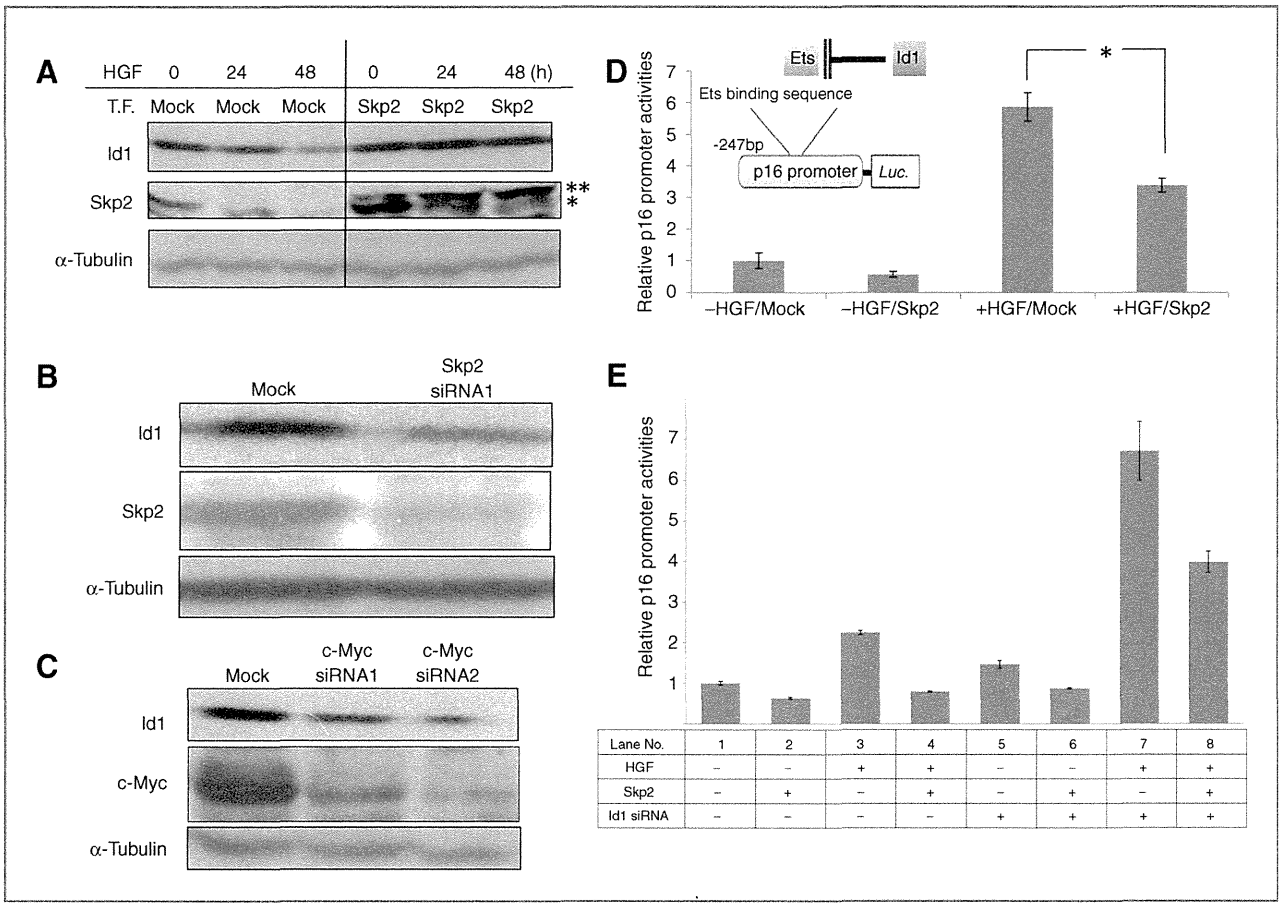

Figure 6. Skp2 regulates Id1 expression through Myc activation. A, Western blot analysis to assess the effect of high expression of Skp2 on endogenous Id1 expression. Endogenous and exogenous Skp2 were detected with anti-Skp2 antibody and their positions are indicated with * and **, respectively. The result is representative of three independent experiments. B and C, Western blot analysis to assess effect of Skp2 knockdown (B) or c-Myc knockdown (C) on endogenous Id1 expression. Two kinds of siRNA targeting Skp2 (B and Supplementary Fig. S7) or c-Myc (C) were used. Cell lysates were prepared at 48 hours after transfection and subjected to immunoblotting. Experiments were carried out at least twice with similar results and representative data are shown (A–C). D, effect of high expression of Skp2 on the p16 promoter. Cells were transfected with a reporter construct encoding the −247 promoter of the *p16* gene fused to the *luciferase* gene together with Skp2. Luciferase activities were determined as described in Materials and Methods. A schematic diagram of the p16 promoter is shown. The average fold-increase in luciferase activity compared with a Mock transfection in the absence of HGF is indicated. Each value represents the mean ± S.D. of triplicate determinants. *, $P < 0.01$; Student *t* test. E, effect of Id1 knockdown on the p16 promoter in cells with high expression of Skp2 in the presence of HGF. Cells were transfected with Id1 siRNA (+) or randomized siRNA (−) as a control. After 24 hours, cells were transfected with the reporter construct together with Skp2 (+) or Mock (−). Luciferase activities were determined as in (D). The average fold-increase in luciferase activity compared with a randomized siRNA and Mock-transfection in the absence of HGF is indicated.

reported that ERK-dependent downregulation of endogenous Skp2 by HGF reduces Myc activity, leading to inhibition of HepG2 hepatoma cell proliferation through a decrease in Id1 expression. The downregulation was also confirmed in established tumors from HepG2 cells in mice. Our data reveal a mechanism by which HGF suppresses cell proliferation through Skp2 downregulation. Our data suggested that Skp2 is physiologically involved in the regulation of Myc activity as its activator independently of its role in ubiquitination, but not in the regulation of p27 degradation. In addition, a hepatoma cell line other than HepG2, HuH7, proliferation of which is also suppressed by HGF in an ERK-dependent manner, also showed ERK-dependent downregulation of Skp2 (Fig. 1D) and Id1 (Supplementary Fig. S6), suggesting that some other cancer cells arrest their proliferation by HGF through Skp2 downregulation in the SCF-independent manner.

Myc regulates the transcription of various genes responsible for controlling cell proliferation, the cell cycle, transcription, cell motility and so on, leading to the initiation, promotion, and progression of a wide range of cancers (32). Among the targets of Myc, we found in this study that expression of Id1 is regulated by Myc through Skp2 (Fig. 6). A comprehensive analysis to find Myc-binding sites in a human genome with ChIP assays showed a binding site in the upstream region of the *Id1* gene (33), supporting regulation of Id1 expression by Myc through Skp2. As we previously showed that Id1 is downregulated by HGF (10), which leads to inhibition of HepG2 cell proliferation, we propose the model displayed in Fig. 7 to illustrate the

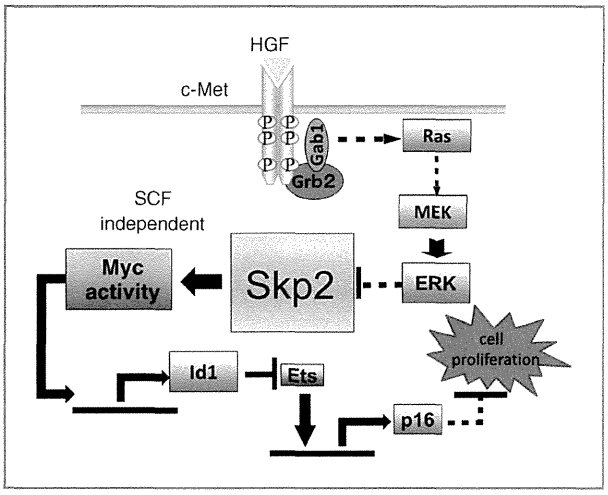

Figure 7. Schematic model of the involvement of Skp2 downregulation in the HGF-induced inhibition of cell proliferation. HGF treatment of the cells downregulates Skp2 expression in an ERK-dependent manner, leading to a reduction in Myc activity. The reduction in Myc activity induces a decrease in Id1, which leads to the activation of a transcription factor, Ets. The activated Ets upregulates p16 expression, which eventually induces inhibition of proliferation in HepG2 hepatoma cells.

involvement of the downregulation of Skp2 in the inhibition of the cell proliferation by HGF. Treatment with HGF downregulates Skp2 expression in an ERK-dependent manner, leading to reduced transcriptional activity of Myc. The reduction in Myc activity decreases Id1 expression, which leads to the activation of a transcription factor, Ets. The activated Ets upregulates p16 expression, which results in inhibition of proliferation in HepG2 hepatoma cells. However, the detailed mechanism of how Skp2 affects Myc activity remains to be elucidated. As Myc activity is generally regulated in the balance of Myc/Max/Mad complexes, we conducted immunoprecipitation assays to analyze the Myc/Max complex, which is the transcription-active form, in the absence or presence of HGF. We found that the amount of Myc/Max complex is not altered even in the presence of HGF (Supplementary Fig. S9), suggesting that Skp2 affects Myc activity not through disruption of the balance of the complexes.

It was previously reported that Skp2 activates the transcription factor c-Myc via ubiquitination as a component of SCF^{Skp2}, which leads to the upregulation of a subset of target genes involved in cell proliferation (18, 19). In contrast, a recent report showed that ubiquitination of c-Myc by the SCF complex is not involved in Myc's activation by Skp2, and this activation upregulates a target gene, *RhoA*, in cell invasion, through a novel transcription complex consisting of Myc-Skp2-Miz1-p300 (20). In the present study, our data suggested that Skp2 functions as a transcriptional activator of Myc rather than a component of the SCF complex in HGF signaling in HepG2 cells (Fig. 5). Thus, in addition to the upregulation of RhoA in cell invasion, it is possible that the Myc-Skp2-Miz1-p300 transcription complex is involved in the regulation of cell proliferation through upregulation of Id1 expression.

We showed that Skp2 is downregulated at the mRNA level in an ERK-dependent manner in HepG2 cells treated with HGF (Fig. 1). Previous reports showed that transcription factor E2F regulates Skp2 expression at the mRNA level in an Akt-dependent manner in other types of cells (34). Although it was previously shown that the inhibitory effect of HGF on the proliferation of HepG2 cells is independent of Akt signaling (7), E2F seemed to be a candidate transcription factor responsible for the Skp2 expression in HGF signaling, because we found that HGF treatment of HepG2 cells reduces the levels of E2F1, and E2F activity (data not shown). To address whether E2F regulates Skp2 expression in HGF signaling, we constructed another HepG2 cell line, in which E2F1 is induced by addition of IPTG. Induction of E2F1 was successfully activated an E2F-responsive promoter, but had no effect on Skp2 expression (data not shown). This result indicated that the regulatory mechanism of Skp2 downregulation induced by HGF is different from that in Akt signaling.

It is generally recognized that the amount of p27 protein, which is predominantly regulated by degradation through ubiquitination by SCF^{Skp2}, is responsible for the suppression of cell proliferation (14). The effect of p27 on the proliferation of HepG2 cells was shown in a previous report, in which β1-integrin–mediated downregulation of p27 through upregulation of Skp2 accelerated the proliferation (26). As HGF treatment of HepG2 cells upregulates p27 protein, we had expected the upregulation to contribute to the suppression of cell proliferation by HGF. However, in the present study, our data showed that partial inhibition of the strong ERK activation, which restores both the amount of Skp2 and cell proliferation suppressed by HGF, has no effect on the upregulation of p27 induced with HGF (Fig. 1B). Our data also showed that high expression of Skp2 restores the cell proliferation suppressed by HGF without affecting the upregulation of p27 (Fig. 2). These results indicate that the upregulation of p27 does not contribute to the suppression of HepG2 cell proliferation by HGF. Accumulating data suggest that p27 has another role in regulating cell motility and migration independent of its cell-cycle role. p27 increases the stability of actin stress fibers by binding to and inhibiting RhoA in cytoplasm, which results in an increase in cell motility (35). As HGF treatment increases the motility of HepG2 cells, leading to cell scattering, the upregulation of p27 might contribute to the increased cell motility with HGF. The significance of the upregulation of p27 expression in HepG2 cells treated with HGF remains to be elucidated.

It was previously shown that the overexpression of Myc in the liver induces the formation of hepatocellular tumors (36, 37), and its inactivation results in regression of the tumors and differentiation of the tumor cells into normal liver cells such as hepatocytes (21), indicating the importance of Myc activity for hepatocarcinogenesis. Accumulating evidence also indicates an important role for Myc activation in the progression of hepatomas (22, 38, 39). We showed here that endogenous Myc activity is regulated by Skp2 in a hepatoma cell line. Thus, it is likely that Skp2 has an important role in

hepatocarcinoma through the regulation of Myc activity. Another report suggested suppression of Myc-induced hepatocarcinogenesis by HGF: hepatocarcinogenesis was induced in transgenic mice expressing c-Myc, but not in transgenic mice expressing c-Myc in combination with HGF (40). The suppression might be caused by downregulation of Skp2. While we showed that HGF treatments of two hepatoma cell lines, HepG2 and HuH7, downregulate Skp2 mRNA in the presence of HGF, further studies of Skp2 in liver tumors and other hepatoma cells would be required to elucidate the involvement of Skp2 in Myc-induced hepatocarcinogenesis, and its suppression via downregulation of Skp2.

Disclosure of Potential Conflicts of Interest

No potential conflicts of interest were disclosed.

Authors' Contributions

Conception and design: T. Tanaka
Development of methodology: Y. Inagaki
Acquisition of data (provided animals, acquired and managed patients, provided facilities, etc.): X. Li, Y. Takizawa, T. Hashimoto, Y. Inagaki, M. Komada, T. Tanaka
Analysis and interpretation of data (e.g., statistical analysis, biostatistics, computational analysis): X. Li, Y. Bian, T. Tanaka
Writing, review, and/or revision of the manuscript: M. Komada, T. Tanaka
Administrative, technical, or material support (i.e., reporting or organizing data, constructing databases): T. Tanaka
Study supervision: T. Ikoma, J. Tanaka, N. Kitamura, M. Komada, T. Tanaka

Acknowledgments

The authors thank Dr. Eiji Hara for allowing us to use the -247 promoter. The authors also thank Mr. Takahito Nakayama and Ms. Hiroko Shirai for supporting our experiments and for information on the Id1 promoter, respectively.

Grant Support

This work was supported by Grants-in-aid for Scientific Research (No. 19570124 and No. 22570137; to T.Tanaka, No. 24241044; to T.Ikoma) from the Japan Society for the Promotion of Science.

The costs of publication of this article were defrayed in part by the payment of page charges. This article must therefore be hereby marked *advertisement* in accordance with 18 U.S.C. Section 1734 solely to indicate this fact.

Received December 29, 2012; revised May 1, 2013; accepted May 17, 2013; published OnlineFirst October 30, 2013.

References

1. Zarnegar R, Michalopoulos GK. The many faces of hepatocyte growth factor: from hepatopoiesis to hematopoiesis. J Cell Biol 1995;129:1177–80.
2. Ma PC, Maulik G, Christensen J, Salgia R. c-Met: structure, functions and potential for therapeutic inhibition. Cancer Metast Rev 2003;22:309–25.
3. Tajima H, Matsumoto K, Nakamura T. Hepatocyte growth factor has potent anti-proliferative activity in various tumor cell lines. FEBS Lett 1991;291:229–32.
4. Shiota G, Rhoads DB, Wang TC, Nakamura T, Schmidt EV. Hepatocyte growth factor inhibits growth of hepatocellular carcinoma cells. Proc Natl Acad Sci U S A 1992;89:373–7.
5. Furge KA, Zhang Y-W, Vande Woude GF. Met receptor tyrosine kinase: enhanced signaling through adapter proteins. Oncogene 2000;19:5582–9.
6. Nakanishi K, Fujimoto J, Ueki T, Kishimoto K, Hashimoto-Tamaoki T, Furuyama J, et al. Hepatocyte growth factor promotes migration of human hepatocellular carcinoma via phosphatidylinositol 3-kinase. Clin Exp Metastas 1999;17:507–14.
7. Tsukada Y, Miyazawa K, Kitamura N. High intensity ERK signal mediates hepatocyte growth factor-induced proliferation inhibition of the human hepatocellular carcinoma cell line HepG2. J Biol Chem 2001;276:40968–76.
8. Tsukada Y, Tanaka T, Miyazawa K, Kitamura N. Involvement of down-regulation of Cdk2 activity in hepatocyte growth factor-induced cell cycle arrest at G1 in the human hepatocellular carcinoma cell line HepG2. J Biochem 2004;136:701–9.
9. Han J, Tsukada Y, Hara E, Kitamura N, Tanaka T. Hepatocyte growth factor induces redistribution of p21(CIP1) and p27(KIP1) through ERK-dependent p16(INK4a) up-regulation, leading to cell cycle arrest at G1 in HepG2 hepatoma cells. J Biol Chem 2005;280:31548–56.
10. Ushio K, Hashimoto T, Kitamura N, Tanaka T. Id1 is down-regulated by hepatocyte growth factor via ERK-dependent and ERK-independent signaling pathways, leading to increased expression of $p16^{Ink4a}$ in hepatoma cells. Mol Cancer Res 2009;7:1179–88.
11. Zheng N, Schulman BA, Song L, Miller JJ, Jeffrey PD, Wang P, et al. Structure of the Cul1-Rbx1-Skp1-F boxSkp2 SCF ubiquitin ligase complex. Nature 2002;416:703–9.
12. Frescas D, Pagano M. Deregulated proteolysis by the F-box proteins Skp2 and beta-TrCP: tipping the scales of cancer. Nat Rev Cancer 2008;8:438–49.
13. Carrano AC, Eytan E, Hershko A, Pagano M. Skp2 is required for the ubiquitin-mediated degradation of the Cdk-inhibitor p27. Nat Cell Biol 1999;1:193–9.
14. Sutterluty H, Chatelain E, Marti A, Wirbelauer C, Senften M, Müller U, et al. p45/Skp2 promotes p27/Kip1 degradation and induces S phase in quiescent cells. Nat Cell Biol 1999;1:207–14.
15. Gstaiger M, Jordan R, Lim M, Catzavelos C, Mestan J, Slinger-land J, et al. Skp2 is oncogenic and overexpressed in human cancers. Proc Natl Acad Sci U S A 2001;98:5043–8.
16. Latres E, Chiarle R, Schulman BA, Pavletich NP, Pellicer A, Inghirami G, et al. Role of the F-box protein Skp2 in lymphomagenesis. Proc Natl Acad Sci U S A 2001;98:2515–20.
17. Oliveira AA, Okuno SH, Nascimento AG, Lloyd RV. Skp2 protein expression in soft tissue sarcomas. J Clin Oncol 2003;21:722–7.
18. Kim SY, Herbst A, Tworkowski KA, Salghetti SE, Tansey WP. Skp2 regulates Myc protein stability and activity. Mol Cell 2003;11:1177–88.
19. von der Lehr N, Johansson S, Wu S, Bahram F, Castell A, Cetinkaya C, et al. The F-box protein Skp2 participates in c-Myc proteosomal degradation and acts as a cofactor for c-Myc-regulated transcription. Mol Cell 2003;11:1189–200.
20. Chan CH, Lee SW, Li CF, Wang J, Yang WL, Wu CY, et al. Deciphering the transcriptional complex critical for RhoA gene expression and cancer metastasis. Nat Cell Biol 2010;12:457–67.
21. Shachaf CM, Kopelman AM, Arvanitis C, Karlsson A, Beer S, Mandl S, et al. Myc inactivation uncovers pluripotent differentiation and tumour dormancy in hepatocellular cancer. Nature 2004;431:1112–7.
22. Kaposi-Novak P, Libbrecht L, Woo HG, Lee YH, Sears NC, Coulouarn C, et al. Central role of c-Myc during malignant conversion in human hepatocarcinogenesis. Cancer Res 2009;69:2775–82.
23. Tanaka T, Kubota M, Shinohara K, Yasuda K, Kato J-Y. *In vivo* analysis of the cyclin D1 promoter during early embryogenesis in *Xenopus*. Cell Stuct Funct 2003;28:165–77.
24. Shirako E, Hirayama N, Tsukada Y, Tanaka T, Kitamura N. Up-regulation of $p21^{CIP1}$ expression mediated by ERK-dependent and –independent pathways contributes to hepatocyte growth factor induced inhibition of HepG2 hepatoma cell proliferation. J Cell Biochem 2008;104:176–88.
25. Kondo A, Hirayama N, Sugito Y, Shono M, Tanaka T, Kitamura N. Coupling of Grb2 to Gab1 mediates hepatocyte growth factor-induced high Intensity ERK signalrequired for inhibition of HepG2 hepatoma cell proliferation. J Biol Chem 2008;283:1428–36.
26. Zhang H, Ozaki I, Mizuta T, Yoshimura T, Matsuhashi S, Hisatomi A, et al. Mechanism of beta 1-integrin-mediated hepatoma cell growth

involves p27 and S-phase kinase-associated protein 2. Hepatology 2003;38:305–13.
27. Zhao Y, Jian W, Gao W, Zheng YX, Wang YK, Zhou ZQ, et al. RNAi silencing of c-Myc inhibits cell migration, invasion, and proliferation in $HepG_2$ human hepatocellular carcinoma cell line: c-Myc silencing in hepatocellular carcinoma cell. Cancer Cell Int 2013;13:23.
28. Hann SR, Eisenman RN. Proteins encoded by the human c-myc oncogene: differential expression in neoplastic cells. Mol Cell Biol 1984;4:2486–97.
29. Grandori C, Cowley SM, James LP, Eisenman RN. The Myc/Max/Mad network and the transcriptional control of cell behavior. Annu Rev Cell Dev Biol 2000;16:653–99.
30. Swarbrick A, Akerfeldt MC, Lee CS, Sergio CM, Caldon CE, Hunter LJ, et al. Regulation of cyclin expression and cell cycle progression in breast epithelial cells by the helix-loop-helix protein Id1. Oncogene 2005;24:381–9.
31. Geng H, Rademacher BL, Pittsenbarger J, Huang CY, Harvey CT, Lafortune MC, et al. Id1 enhances docetaxel cytotoxicity in prostate cancer cells through inhibition of p21. Cancer Res 2010;70: 3239–48.
32. Vita M, Henriksson M. The Myc oncoprotein as a therapeutic target for human cancer. Semin Cancer Biol 2006;16:318–30.
33. Zeller KI, Zhao XD, Lee CWH, Chiu KP, Yao F, Yustein JT, et al. Global mapping of c-Myc binding sites and target gene networks in human B cells. Proc Natl Acad Sci U S A 2006;103:17834–9.
34. Reichert M, Saur D, Hamacher R, Schmid RM, Schneider G. Phosphoinositide-3-kinase signaling controls S-phase kinase-associated protein 2 transcription via E2F1 in pancreatic ductal adenocarcinoma cells. Cancer Res 2007;67:4149–56.
35. Larrea MD, Wander SA, Slingerland JM. p27 as Jekyll and Hyde: regulation of cell cycle and cell motility. Cell Cycle 2009;8:3455–61.
36. Sandgren EP, Quaife CJ, Pinkert CA, Palmiter RD, Brinster RL. Oncogene-induced liver neoplasia in transgenic mice. Oncogene 1989;4: 715–24.
37. Murakami H, Sanderson ND, Nagy P, Marino PA, Merlino G, Thorgeirsson SS. Transgenic mouse model for synergistic effects of nuclear oncogenes and growth factors in tumorigenesis: interaction of c-myc and transforming growth factor alpha in hepatic oncogenesis. Cancer Res 1993;53:1719–23.
38. Saddic LA, Wirt S, Vogel H, Felsher DW, Sage J. Functional interactions between retinoblastoma and c-Myc in a mouse model of hepatocellular carcinoma. PLos ONE 2011;6:e19758.
39. Zimonjic DB, Popescu NC. Role of Dlc1 tumor suppressor gene and Myc oncogene in pathogenesis of human hepatocellular carcinoma: potential prospects for combined targeted therapeutics. Int J Oncol 2012;41:393–406.
40. Santoni-Rugiu E, Preisegger KH, Kiss A, Audolfsson T, Shiota G, Schmidt EV, et al. Thorgeirsson S.S. Inhibition of neoplastic development in the liver by hepatocyte growth factor in a transgenic mouse model. Proc Natl Acad Sci U S A 1996;93:9577–82.

The American Journal of Pathology, Vol. 183, No. 3, September 2013

ELSEVIER

The American Journal of
PATHOLOGY

ajp.amjpathol.org

CARDIOVASCULAR, PULMONARY, AND RENAL PATHOLOGY

Qualitative Rather than Quantitative Changes Are Hallmarks of Fibroblasts in Bleomycin-Induced Pulmonary Fibrosis

Tatsuya Tsukui,*† Satoshi Ueha,*† Jun Abe,*† Shin-ichi Hashimoto,*† Shigeyuki Shichino,*† Takeshi Shimaoka,*† Francis H.W. Shand,‡ Yasuka Arakawa,*† Kenshiro Oshima,§ Masahira Hattori,§ Yutaka Inagaki,†¶ Michio Tomura,‖ and Kouji Matsushima*†

From the Department of Molecular Preventive Medicine, Graduate School of Medicine, University of Tokyo, Tokyo, Japan; the Japan Science and Technology Agency—CREST Program,† Tokyo, Japan; the Department of Pharmacology,‡ University of Melbourne, Parkville, Australia; the Department of Computational Biology,§ Graduate School of Frontier Sciences, University of Tokyo, Chiba, Japan; the Research Unit for Tissue Remodeling and Regeneration,¶ Tokai University School of Medicine, Kanagawa, Japan; and the Center for Innovation in Immunoregulative Technology and Therapeutics,‖ Kyoto University Graduate School of Medicine, Kyoto, Japan*

Accepted for publication June 3, 2013.

Address correspondence to Kouji Matsushima, M.D., Ph.D., Department of Molecular Preventive Medicine, Graduate School of Medicine, The University of Tokyo, 7-3-1, Hongo, Bunkyo-ku, Tokyo 113-0033, Japan. E-mail: koujim@m.u-tokyo.ac.jp.

Pulmonary fibrosis is characterized by accumulation of activated fibroblasts that produce excessive amounts of extracellular matrix components such as collagen type I. However, the dynamics and activation signatures of fibroblasts during fibrogenesis remain poorly understood, especially *in vivo*. We examined changes in lung tissue cell populations and in the phenotype of activated fibroblasts after acute injury in a model of bleomycin-induced pulmonary fibrosis. Despite clustering of collagen type I-producing fibroblasts in fibrotic regions, flow cytometry-based quantitative analysis of whole lungs revealed that the number of fibroblasts in the lungs remained constant. At the peak of inflammation, fibroblast proliferation and apoptosis were both increased, suggesting that the clustering was not merely a result of proliferation, but also of fibroblast migration from nearby alveolar walls. Parabiosis experiments demonstrated that fibroblasts were not supplied from the circulation. Comprehensive gene expression analysis of freshly isolated fibroblasts revealed a detailed activation signature associated with fibrogenesis, including changes in genes responsible for migration and extracellular matrix construction. The *Spp1* gene, which encodes osteopontin, was highly up-regulated and was an identifying characteristic of activated fibroblasts present at the sites of remodeling. Osteopontin may serve as a useful marker of profibrotic fibroblasts. These results provide insights into the cellular and molecular mechanisms underlying pulmonary fibrosis and provide a foundation for development of specific antifibrotic therapies. *(Am J Pathol 2013, 183: 758–773; http://dx.doi.org/10.1016/j.ajpath.2013.06.005)*

Fibrosis is a common pathological feature of chronic inflammation. In response to injury, activated fibroblasts accumulate in damaged tissue and irreversibly deposit excessive amounts of extracellular matrix (ECM) components, which severely impair organ function.[1] In the lungs, the most common fibrotic disease is idiopathic pulmonary fibrosis, which is characterized by a histological pattern of usual interstitial pneumonia including bronchiolization and honeycombing. Because means for early diagnosis and effective therapies are lacking for idiopathic pulmonary fibrosis, patients have a median survival of only 2.5 to 3.5 years after diagnosis.[2]

Within fibrotic lesions, fibroblastic cells are activated by cytokines and growth factors such as TGF-β, often expressing α-smooth muscle actin (α-SMA) and adopting a myofibroblast phenotype. As the major producers of ECM components such as collagen type I, myofibroblasts play a central role in the pathogenesis of fibrosis.[3,4] Myofibroblasts derive from several types of progenitor cells, depending on the organ and experimental model. Although resident fibroblasts have been considered the major progenitors of myofibroblasts in the lungs, the extent of the contribution of other cell populations, such as epithelial cells or fibrocytes, remains a matter of debate.[5–8] Hoyles et al[9] found that resident fibroblast-specific deletion of the high-affinity type II TGF-β receptor attenuated bleomycin-induced lung fibrosis,

Supported by the Japan Science and Technology Agency (CREST Program).

http://dx.doi.org/10.1016/j.ajpath.2013.06.005

demonstrating the important role of resident fibroblasts in their model. Rock et al[10] recently used genetic lineage labeling to demonstrate that type II alveolar cells and Scgb1a1-positive cells (mainly bronchiolar Clara cells) in the alveoli and bronchioles did not become myofibroblasts through epithelial–to-mesenchymal transition in bleomycin-induced lung fibrosis. They also showed that NG2-expressing pericyte-like cells (which are sources of myofibroblasts in some fibrosis models[11,12]) were not major progenitors of myofibroblasts in the lungs. Nonetheless, there remains a need to clarify the role of resident fibroblasts as myofibroblast progenitors in the lungs.

Resident fibroblasts, which comprise 30% to 40% of tissue cells in the lungs, form scaffolds for alveoli by secreting ECM components.[13] Despite the prevalence of these cells in the alveoli and despite their postulated roles in pulmonary fibrosis, the *in vivo* properties of resident fibroblasts in both their normal and activated states remain poorly understood. Fibroblasts lack specific surface markers, and stromal cell heterogeneity in lung has not been well characterized. Earlier studies have often isolated fibroblasts by their adhesiveness to plastic dishes, which in itself can affect the phenotype of fibroblasts.[14] In addition, the histological approaches that are commonly used in fibrosis studies have limited parameters and resolution for the quantitative analysis of single cells. For these reasons, it remains largely unknown how fibroblasts generate fibrotic lesions and contribute to organ fibrosis. To develop novel therapies for pulmonary fibrosis that specifically suppress fibroblast activation, accumulation, and ECM deposition, a more detailed picture of how these processes occur is required.

In the present study, we analyzed qualitative and quantitative changes in fibroblast populations in a model of bleomycin-induced lung fibrosis. Fibroblasts were identified using collagen type I, alpha 2 (*Col1a2*) reporter mice, in which collagen type I-expressing fibroblasts are labeled with EGFP.[15,16] Flow-cytometric analysis of cells from enzymatically dissociated lung tissue taken during bleomycin-induced lung fibrosis revealed phenotypic changes without a change in overall fibroblast numbers. Although fibroblast proliferation increased, this was countered by a similar increase in apoptosis. On the other hand, gene expression profiles of freshly isolated fibroblasts generated by next-generation DNA sequencing revealed a detailed gene signature for profibrotic cells. Specifically, the gene encoding osteopontin (OPN) was highly up-regulated, suggesting that OPN may serve as an activation marker of lung fibroblasts.

Materials and Methods

Mice

Col1a2-GFP (C57BL/6 background for $\geq$10 generations) and ROSA-CAG-SCAT3.1 mice were generated in previous studies.[16,17] ROSA-CAG-SCAT3.1 mice were generated with BDF1-derived ES cells and backcrossed to C57BL/6 mice for at least two generations.[17] The properties of FucciG1-#639 and FucciS/G2/M-#474 mice (both C57BL/6 background) are to be published elsewhere. C57BL6/J mice were purchased from Japan SLC (Hamamatsu, Japan) or CLEA Japan (Tokyo, Japan). Animal experiments were performed on 6- to 12-week–old mice. Mice were bred and maintained in specific pathogen-free facilities at the University of Tokyo. All animal experiments were performed in accordance with the guidelines of the Animal Care and Use Committee of the University of Tokyo.

Intratracheal Instillation

Mice were anesthetized with pentobarbital. Bleomycin sulfate (1.25 to 2.5 mg/kg dissolved in 50 μL of saline solution; Toronto Research Chemical, Toronto, ON, Canada) or 50 μg lipopolysaccharide from *Salmonella minnesota* R595 (Enzo Life Sciences, Farmingdale, NY) were instilled intratracheally by oropharyngeal aspiration.[18]

BrdU

Bromodeoxyuridine (BrdU; 0.8 mg in 200 μL saline; Sigma-Aldrich, Tokyo, Japan; St. Louis, MO) was injected intraperitoneally at 24 hours before sacrifice. Mouse drinking water was supplemented with 0.8 mg/mL BrdU for this 24-hour period. For long-term BrdU pulse experiments, mice were injected with 0.8 mg BrdU i.p. after bleomycin treatment and given 0.8 mg/mL BrdU-containing drinking water until analysis.

Tissue Dissociation

Mice were anesthetized with pentobarbital. After perfusion with 5 mL of PBS via the right ventricle, the trachea was cannulated. Pulmonary airspaces were lavaged three times with 1 mL PBS each time. Either the left or right lobes of the lungs were harvested for flow cytometry. The lobes were cut into small pieces and digested in protease solution [0.2% collagenase (Wako Pure Chemical Industries, Osaka, Japan), 0.1 mg/mL Dispase II (Roche, Basel, Switzerland), and 2000 U/mL DNase I (Merck, Darmstadt, Germany) in RPMI medium (Sigma-Aldrich)] for 60 minutes at 37°C with trituration by micropipette every 20 minutes. After being passed through a 70-μm strainer (BD Biosciences, San Diego, CA), cells were washed and resuspended in RPMI medium (Sigma-Aldrich) containing 10% fetal bovine serum. Peripheral blood cells were treated with red blood cell lysis buffer before analysis by flow cytometry.

Hydroxyproline Assay

Lung hydroxyproline content was measured as described previously.[19,20] In brief, mice were sacrificed and the left lungs were harvested. The lungs were minced and suspended in up to 800 μL of ultrapure water, after which 800 μL of

12 N HCl was added and the mixture heated for 24 hours at 110°C. The resulting acid hydrolysates was filtrated through a 0.45-μm filter, and 25 μL was transferred to new tubes. Next, 25 μL of 6 N NaOH, 50 μL of citric acetate buffer (5% citric acid, 7.24% sodium acetate, 3.4% NaOH, 1.2% glacial acetic acid, pH 6.0), and 400 μL of chloramine T solution (564 mg of chloramine T, 4 mL of H_2O, 4 mL of *n*-propanol, and 32 mL of citric-acetate buffer) were added, and the mixture was incubated for 20 minutes at room temperature. Next, 400 μL of Ehrlich's solution (4.5 g of 4-dimethylaminobenzaldehyde, 18.6 mL of *n*-propanol, and 7.8 mL of 70% perchloric acid) was added, and the mixture was incubated for a further 15 minutes at 65°C before the absorbance (optical density OD_{550}) of the solution was measured. The reagents were purchased from Wako Pure Chemical Industries, Sigma-Aldrich Japan, and Tokyo Chemical Industry (Tokyo, Japan).

Flow Cytometry

Cell suspensions were incubated with anti-CD16/32 antibody to block nonspecific binding, followed by PerCP-Cy5.5 anti-CD31, phycoerythrin (PE)-Cy7 anti-EpCAM, and allophycocyanin (APC)-Cy7 anti-Ter119 antibodies from Biolegend (San Diego, CA) and APC anti-CD45.2 antibody from BD Biosciences (San Jose, CA). For α-SMA and cleaved caspase 3 intracellular staining, cells were fixed with Cytofix/Cytoperm buffer (BD Biosciences) for 20 minutes before incubation with APC anti-α-SMA antibody (R&D Systems, Minneapolis, MN) and anti-cleaved caspase 3 (Cell Signaling Technology, Danvers, MA), followed by incubation with Alexa Fluor 647 anti-rabbit IgG (Life Technologies, Tokyo, Japan; Carlsbad, CA) for cleaved caspase 3. BrdU incorporation was examined using a BrdU flow kit (BD Biosciences). For intracellular OPN staining, single-cell suspensions were cultured in 10% fetal bovine serum–RPMI medium (Sigma-Aldrich) at 37°C with or without the protein transport inhibitor brefeldin A (BFA) for 6 hours, after which adherent cells were collected using trypsin–EDTA. After a washing, the cells were fixed with Cytofix/Cytoperm buffer (BD Biosciences) and then stained with goat anti-OPN primary antibodies (R&D Systems), followed by Alexa Fluor 647 anti-goat IgG as secondary antibody (Life Technologies). Antibody-labeled cells were washed twice before analysis with a Gallios flow cytometer (Beckman Coulter, Brea, CA). For analysis of cells from SCAT3.1 mice, the FL10 filter was switched to 525BP. Cell sorting was performed on FACSAria (BD Biosciences). Flow cytometry data were analyzed using FlowJo version 7.6.5 software (Tree Star, Ashland, OR).

Immunohistochemistry

Lungs were fixed with 4% paraformaldehyde–PBS for 6 hours at 4°C, treated with 30% sucrose for cryoprotection, and then embedded in TissueTek optimal cutting temperature compound (Sakura Finetek Japan, Tokyo, Japan). For OPN staining, lungs were filled through the trachea with BFA containing 10% fetal bovine serum-RPMI medium (Sigma-Aldrich) and were incubated in the same medium at 37°C for 6 hours, before paraformaldehyde fixation. Frozen sections (6 μm thick) were stained with PE anti-EpCAM (Bio-Legend), APC anti–α-SMA (R&D Systems), anti-collagen type I (Cosmo Bio, Tokyo, Japan), anti-CD45 (BD Biosciences), and anti-OPN (R&D Systems) primary antibodies, followed by incubation with Alexa Fluor 647 anti-rabbit IgG for collagen type I, Alexa Fluor 546 anti-rat IgG for CD45, and Alexa Fluor 647 anti-goat IgG for OPN (Life Technologies). For BrdU staining, sections were incubated in 500 U/mL DNase (Calbiochem; EMD Millipore, Billerica, MA) solution for 60 minutes at 37°C to retrieve the antigen before staining. Sections were mounted with ProLong Gold antifade reagent (Life Technologies), in some cases containing 2 μg/mL propidium iodide (PI). Sections were photographed using an SP5 confocal microscope (Leica Microsystems, Wetzlar, Germany).

SAGE

Gene expression analysis was performed using serial analysis of gene expression (SAGE) and next-generation sequencing with an Ion Torrent Personal Genome Machine (PGM) sequencer (Life Technologies). Lung tissue single-cell suspensions from three mice were pooled for each group, and lineage-negative (Lin^-) GFP^+ fibroblasts were isolated by cell sorting. RNA was isolated from these cells using a *mir*Vana miRNA isolation kit (Life Technologies). The next-generation sequencing data were generated from 1 μg of total RNA. SAGE libraries were constructed using a SOLiD SAGE kit (Life Technologies) according to the manufacturer's protocol. DNA was recovered from the agarose gel using a PureLink gel extraction kit (Life Technologies). DNA fragments of SAGE construct were analyzed on an Agilent 2100 Bioanalyzer platform using a high-sensitivity kit (Agilent Technologies, Santa Clara, CA). Template preparation, emulsion PCR, and Ion Sphere particle enrichment was performed using an Ion Xpress Template kit (Life Technologies) according to the manufacturer's instructions. The quality of the resultant Ion Sphere particle was assessed using a Qubit 2.0 fluorometer (Life Technologies) before the particles were loaded onto a 318 chip (Life Technologies) for sequencing. Raw data from these experiments have been deposited in the NCBI Gene Expression Omnibus (*http://www.ncbi.nlm.nih.gov/geo*; accession number GSE42564).

Mapping of Next-Generation Sequencing Data

For each sample, raw reads from the PGM sequencer were aligned against mouse RefSeq genes (*http://hgdownload.cse.ucsc.edu/goldenpath/mm9/database*) using Burrows-Wheeler alignment software, version 0.6.2, which uses the 25_1 mapping parameter. We generated unique gene counts

by excluding reads that mapped to contigs of more than one gene; reads mapping to several contigs within an isogroup were counted only once. To include only highly expressed genes and to avoid high dispersion, genes with fewer than 50 tags in both saline-treated and bleomycin-treated groups were eliminated from the library before analysis. Gene ontology (GO) analysis was performed using DAVID (Database for Annotation, Visualization and Integrated Discovery) Bioinformatic Resources software version 6.7 (*http://david.abcc.ncifcrf.gov/home.jsp*).[21] Pathway analysis was performed using IPA software version 9.0 (Ingenuity Systems, Redwood City, CA).

qPCR Analysis

A portion of the mRNA isolated for SAGE was reverse-transcribed to cDNA using a Life Technologies high-capacity reverse transcription kit. Quantitative real-time PCR (qPCR) analysis was performed using SYBR Green detection of amplified products and an ABI 7500 real-time PCR system (Life Technologies). Primers used for qPCR were as follows: GAPDH forward 5′-AGTATGACTCCACTCACGGCAA-3′ and reverse 5′-TCTCGCTCCTGGAAGATGGT-3′; Spp1 forward 5′-GGAGGAAACCAGCCAAGG-3′ and reverse 5′-TGCCAGAATCAGTCACTTTCAC-3′; α-SMA forward 5′-CTGGAGAAGAGCTACGAACTGC-3′ and reverse 5′-CTGATCCACATCTGCTGGAAGG-3′; S100a4 forward 5′-GGAGCTGCCTAGCTTCCTG-3′ and reverse 5′-TCCTGGAAGTCAACTTCATTGTC-3′; Tnc forward 5′-GGGCTATAGAACACCGATGC-3′ and reverse 5′-CATTTAAGTTTCCAATTTCAGGTTC-3′; Fn1 forward 5′-CGGAGAGAGTGCCCCTACTA-3′ and reverse 5′-CGATATTGGTGAATCGCAGA-3′; Ereg forward 5′-TTGACGCTGCTTTGTCTAGG-3′ and reverse 5′-GGATCACGGTTGTGCTGAT-3′; Sfrp1 forward 5′-CAGTTGTGGCTTTTGCATTG-3′ and reverse 5′-GAGGGAAGGGAGAGGGTTC-3′; Pcolce2 forward 5′-CAAATTCAGGCCGAAAAAGT-3′ and reverse 5′-CCACAGTGGGCTTTAGACCT-3′; Gsn forward 5′-CAAAGTCGGGTGTCTGAGG-3′ and reverse 5′-CTTCCCTGCCTTCAGGAAT-3′; and Efemp1 forward 5′-CCACAGGGTTACGAAGTGGT-3′ and reverse 5′-TCATTGGTGGTCTCACATTCA-3′.

Statistical Analysis

Statistical comparisons were performed using unpaired *t*-tests (two-tailed). A P value of <0.05 was considered statistically significant. Data are expressed as means ± SEM.

Results

Characterization of GFP$^+$ Cells in the Lungs of Col1a2-GFP Mice

We first investigated what kinds of cells were labeled with GFP in lungs of Col1a2-GFP reporter mice.[16] Lungs were dissociated with a protease solution and analyzed by multicolor flow cytometry. GFP$^+$ cells comprised a distinct population that was negative for the lineage markers Ter119 (data not shown), CD45, CD31, and EpCAM (Figure 1A). Approximately 70% to 80% of Lin$^-$ GFP$^+$ cells were PDGFRα$^+$; the remainder were PDGFRα$^-$ (Figure 1B). Immunofluorescence imaging of lung sections revealed GFP$^+$ cells to be present in alveolar walls and in peribronchiolar and perivascular regions (Figure 1C). The peribronchiolar and perivascular GFP$^+$ cells also expressed α-SMA, consistent with these being smooth muscle cells (Figure 1C).[15] Alveolar GFP$^+$ cells were located in the interstitium, surrounded by basement membranes manifested by collagen type IV (Figure 1D). Previous studies have demonstrated that alveolar fibroblasts are PDGFRα$^+$, NG2$^-$, α-SMA$^-$, and CD31$^-$,[10,22] a phenotype consistent with that observed in alveolar GFP$^+$ cells. In summary, GFP$^+$ cells in Col1a2-GFP mice comprise a mixed population of alveolar fibroblasts and smooth muscle cells, with alveolar fibroblasts constituting the majority.

Quantitative Analysis of Lung Tissue Cell Dynamics

A prominent characteristic of pulmonary fibrosis is the accumulation of activated fibroblasts/myofibroblasts in fibrotic lesions. This is caused by the migration of fibroblasts into alveolar spaces and their subsequent proliferation.[23] Previous studies have demonstrated BrdU uptake of interstitial cells in fibrotic lesions and enhanced *in vitro* proliferative capacity of fibroblasts from fibrotic organs.[24–26] However, it remains to be shown *in vivo* whether this increase in fibroblast numbers mediates the excessive deposition of ECM during fibrosis.

We used a bleomycin-induced lung fibrosis model in Col1a2-GFP mice to investigate changes that occur in lung tissue cell populations. The extent of lung fibrosis occurring in this model was verified by the measurement of hydroxyproline and the expression of profibrotic genes in whole lungs (Supplemental Figure S1). Numbers of leukocytes and of tissue cells such as endothelial cells, epithelial cells, and fibroblasts were determined by multicolor flow cytometry (Figure 2A). The number of CD45$^+$ leukocytes in the lungs was elevated at days 7 and 14 after bleomycin administration (Figure 2B), which may reflect the infiltration of inflammatory cells. CD31$^+$ endothelial cell numbers did not change significantly after bleomycin administration (Figure 2B). In contrast, EpCAM$^+$ epithelial cells, a population that includes alveolar type II cells, bronchiolar epithelial cells, and possibly alveolar type I cells,[27] markedly decreased after bleomycin treatment (Figure 2B). This probably resulted from the denudation of the epithelium that is induced by bleomycin toxicity. Contrary to expectations, the numbers of Lin$^-$ GFP$^+$ fibroblasts in whole-lung tissue preparations remained constant throughout bleomycin-induced lung fibrosis (Figure 2B). Even at days 14 and 21 after bleomycin administration, which fall within the peak

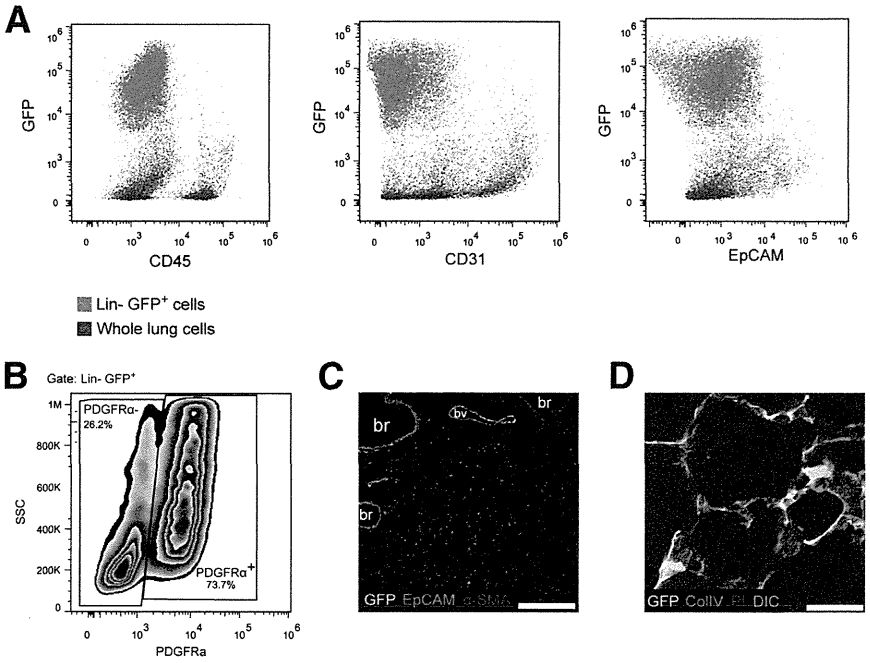

Figure 1 Characterization of GFP$^+$ cells in the lungs of Col1a2-GFP mice. **A:** Lung single-cell suspensions were stained with antibodies against CD45, CD31, and EpCAM. Lin$^-$ (ie, Ter119$^-$ CD45$^-$ CD31$^-$ EpCAM$^-$) GFP$^+$ cells (red) made up a distinctive CD45$^-$ CD31$^-$ EpCAM$^-$ population. **B:** Lin$^-$ GFP$^+$ cells comprised 70% to 80% PDGFRα^+ cells and 20% to 30% PDGFRα^- cells. **C:** Lung sections from Col1a2-GFP mice stained for EpCAM (red) and α-SMA (blue). **D:** Lung sections from Col1a2-GFP mice stained for collagen type IV (red) and PI (blue). Differential interference contrast (DIC) is also shown (gray). Scale bars: 400 μm (**C**); 25 μm (**D**). br, bronchiole; bv, blood vessel.

period for fibrosis,[28] there was no difference in Lin$^-$ GFP$^+$ fibroblast numbers, compared with saline-treated control (Figure 2C), nor was any increase in fibroblast number observed at day 28 (data not shown).

To technically validate these results, we used the lipopolysaccharide-induced acute lung injury model as a negative control in which an increase in fibroblasts is not expected. We observed a massive increase in leukocyte infiltration into the lungs and alveolar air spaces after lipopolysaccharide administration, but the numbers of lung tissue cells including fibroblasts remained unchanged (Supplemental Figure S2). In the absence of a suitable positive control model in which an increase in lung fibroblasts would be expected, we used a tumor lung metastasis model to confirm that increases in lung tissue cells could be detected. At 18 days after intravenous injection of 4×10^6 Lewis lung carcinoma cells (3LL cells), we observed a dramatic increase in EpCAM$^+$ tumor cells without any increase in the other tissue cell populations (Supplemental Figure S3). These results indicate that flow-cytometric analysis after complete digestion of lung tissue is an appropriate way to quantify tissue cell numbers. Thus, the excessive accumulation of ECM that occurs during lung fibrosis cannot be accounted for by an increase in fibroblast numbers.

Qualitative Changes in Fibroblasts after Bleomycin Treatment

Previous studies have shown that exposure of fibroblasts to bleomycin induces an activated phenotype that includes increased α-SMA and collagen type I expression.[4] However, these studies identified fibroblasts only by their stromal localization or by their adhering plastic dishes. Because there was no quantitative increase in fibroblast numbers during fibrosis, we next examined whether there are any phenotypic changes in collagen type I–producing fibroblasts after bleomycin treatment. At day 14, we observed a greater proportion of GFP^{hi} fibroblasts in bleomycin-treated mice, which indicates increased expression of Col1a2 (Figure 3A). GFP^{hi} fibroblasts had high side scatter (SSC) (Figure 3A). Furthermore, many SSC^{hi} fibroblasts had increased forward scatter (FSC) (Figure 3B). Of the bleomycin-treated fibroblasts in the GFP^{hi} SSC^{hi} gate (Figure 3A), 77.3 ± 2.5% also fell into the FSC^{hi} SSC^{hi} gate (Figure 3B), compared with 44.2 ± 2.3% of saline-treated fibroblasts (data not shown) ($P < 0.01$). These data suggest that cell size and intracellular organelle complexity increase in activated fibroblasts. These changes were also quantifiable as greater mean fluorescent intensity values for GFP, SSC, and FSC in Lin$^-$ GFP$^+$ cells from bleomycin-treated mice (Figure 3C).

To investigate whether Lin$^-$ GFP$^+$ fibroblasts differentiate into myofibroblasts, we also measured α-SMA expression by flow cytometry (Figure 3D). In normal lungs (day 0), 4.41 ± 0.49% of Lin$^-$ GFP$^+$ cells were α-SMA$^+$ (Figure 3D), probably representing peribronchiolar and perivascular smooth muscle cells (Figure 3E). At days 7 and 14 after bleomycin administration, the proportion of α-SMA$^+$ cells was almost twice as high as at day 0 (Figure 3D). By day 21, however, the proportion of α-SMA$^+$ cells had returned to normal levels, which is consistent with previous studies.[10,29]

Histological Analysis of Col1a2-GFP Mouse Lungs

Flow-cytometric analysis of fibroblasts revealed clear phenotypic changes associated with activation by bleomycin. We next investigated whether these changes could be observed histologically. In saline-treated lungs, α-SMA expression was confined to peribronchiolar and perivascular

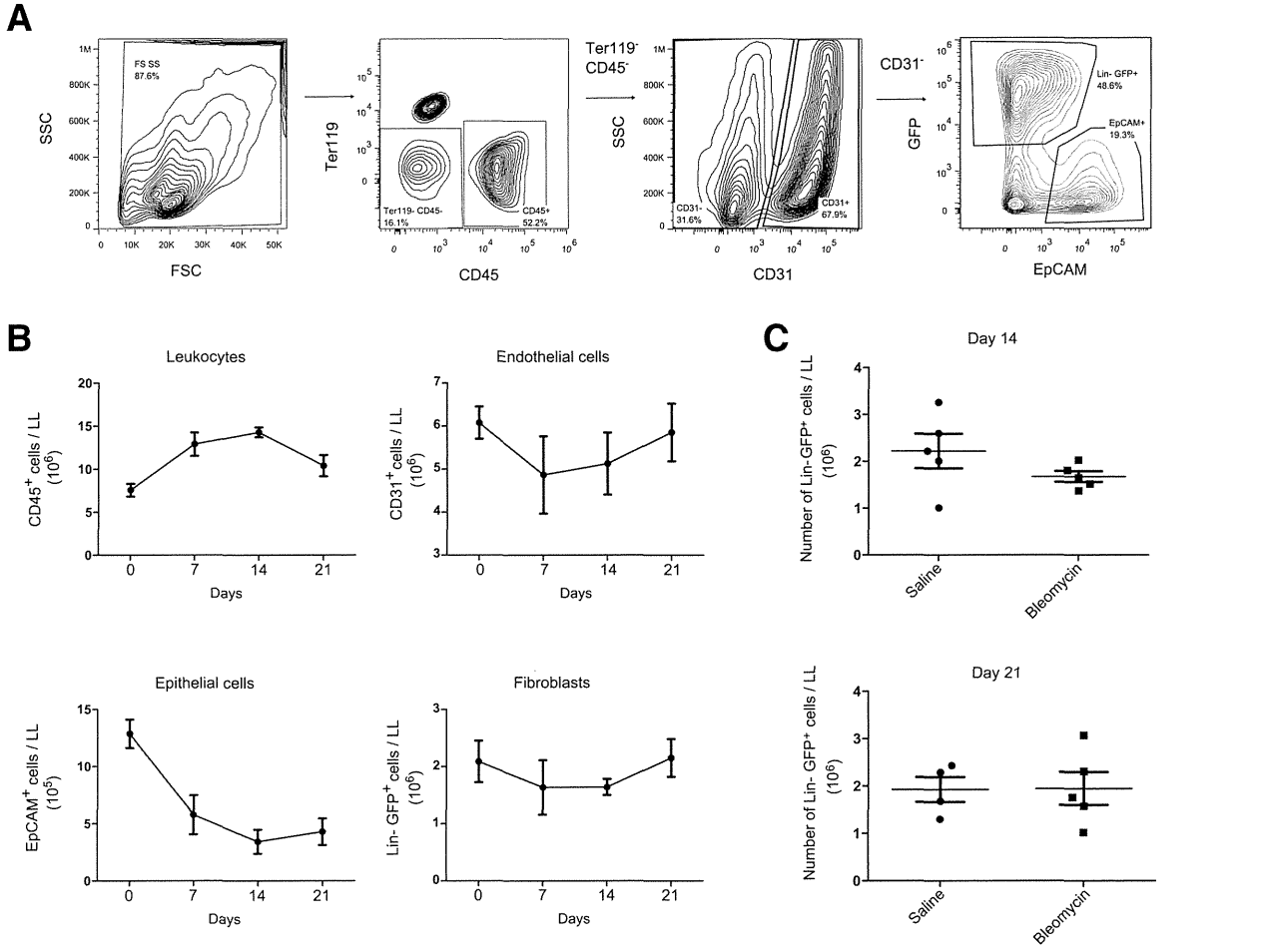

Figure 2 Changes in lung tissue cell populations during bleomycin-induced pulmonary fibrosis. **A:** Enzymatically dissociated lung cells from bleomycin-treated Col1a2-GFP mice were stained for lineage markers and analyzed by flow cytometry. **B:** $CD45^+$ leukocytes, $CD31^+$ endothelial cells, $EpCAM^+$ epithelial cells, and Lin^- GFP^+ fibroblasts were quantified by flow cytometry at 7, 14, and 21 days after bleomycin administration. Day 0 data were from untreated mice. **C:** Numbers of Lin^- GFP^+ cells in the lungs did not differ between saline- or bleomycin-treated mice at 14 and at 21 days after bleomycin administration, as quantified by flow cytometry. Data are expressed as means ± SEM (**B**) or as both means ± SEM and individual data points (**C**). n = 3 or 4 (**B**); 4 or 5 (**C**). LL, left lobe.

smooth muscle cells, with most alveolar fibroblasts negative for α-SMA (Figure 3E). At day 14 after bleomycin treatment, there were a large number of GFP^+ fibroblast clusters (Figure 3E), in which the fibroblasts were surrounded by extracellular collagen type I (Figure 3F). Thus, bleomycin treatment induced the formation of fibrotic regions made up of fibroblast clusters. Many of the GFP^+ fibroblasts in these clusters were α-SMA^+ (Figure 3E), suggesting that these cells were actually myofibroblasts. In bleomycin-treated lungs, α-SMA expression extended beyond the peribronchiolar and perivascular regions into the alveolar region, in accord with the greater numbers of GFP^+ α-SMA^+ cells detected by flow cytometry. The fibroblasts making up the fibrotic regions observed at day 14 after bleomycin treatment had relatively large cell sizes, compared with those in saline-treated lungs (Figure 3E). Taken together with the increase of GFP^+ α-SMA^+ cells detected by flow cytometry (Figure 3D), these results suggest a tendency for GFP^+ alveolar fibroblasts to differentiate into myofibroblasts after bleomycin treatment. These results also suggest that GFP^+ fibroblasts play a central role in the formation of fibrotic regions.

Proliferation and Apoptosis of Fibroblasts after Bleomycin Treatment

Despite lack of change in absolute numbers of lung fibroblasts after treatment with bleomycin, as measured by flow cytometry, GFP^+ fibroblasts in bleomycin-treated lungs displayed clustering and increased cell density in fibrotic regions, which is suggestive of a proliferative response. These conflicting results led us to hypothesize that both proliferation and cell death were accelerated during fibrosis in the lungs, in balance with each other. To examine fibroblast apoptosis, we investigated the activation of caspase 3 using an anti-cleaved caspase 3 antibody (Figure 4A). We treated Col1a2-GFP mice with bleomycin, then measured apoptosis of lung tissue cells by flow cytometry (Figure 4B). Only a very small proportion (0.1% to 0.8%) of endothelial cells were apoptotic during bleomycin-induced fibrosis

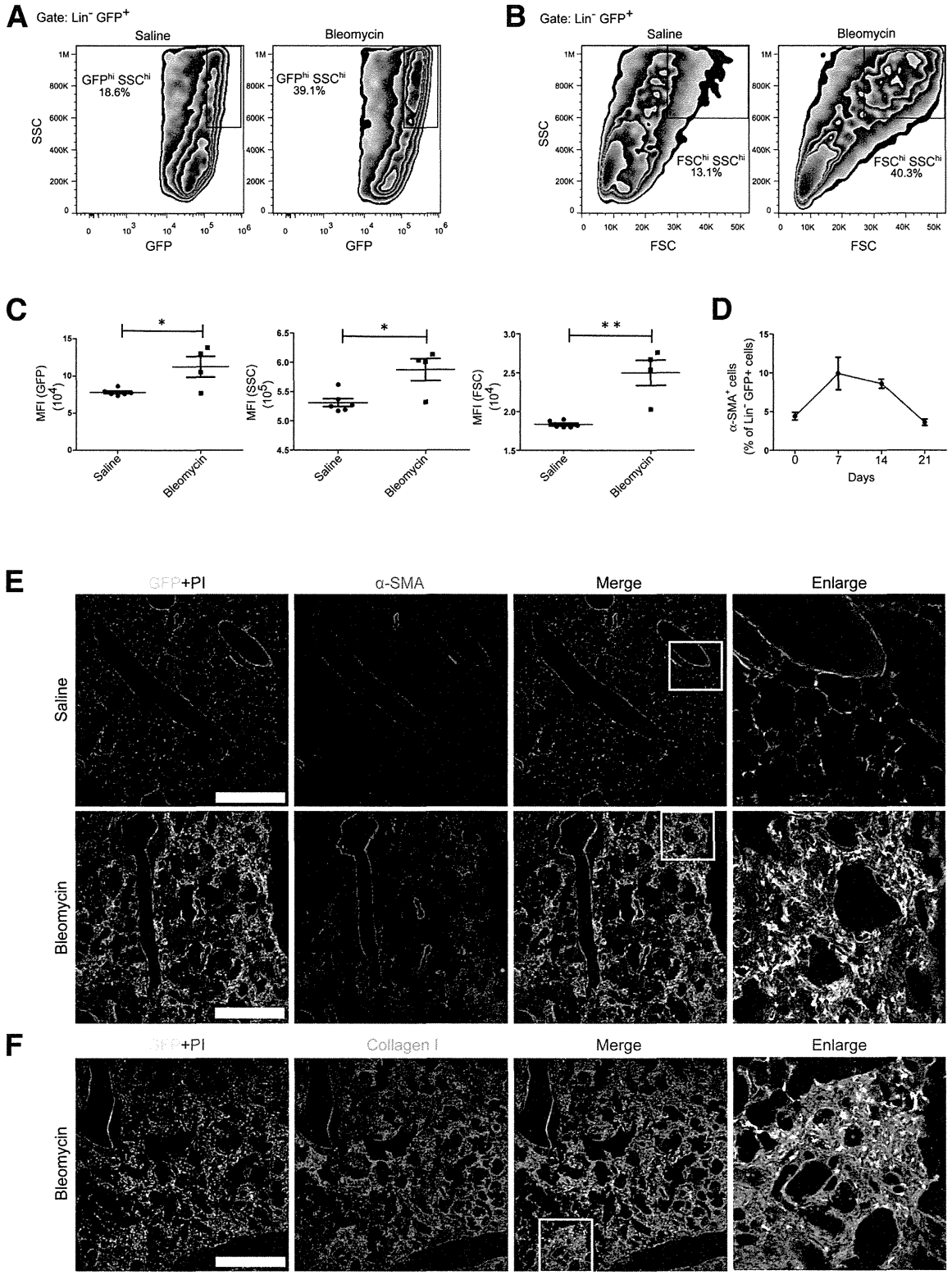

Figure 3 Qualitative changes in fibroblasts during bleomycin-induced lung fibrosis. **A** and **B**: Lung cells from Col1a2-GFP mice at 14 days after saline or bleomycin administration were stained for lineage markers. Lin^- GFP^+ fibroblasts were plotted as SSC versus GFP (**A**) and SSC versus FSC (**B**). **C**: The mean fluorescent intensities (MFI) of GFP, SSC, and FSC signals of Lin^- GFP^+ fibroblasts from Col1a2-GFP mice at 14 days after saline or bleomycin administration. **D**: Lung cells from Col1a2-GFP mice at 0, 7, 14, and 21 days after bleomycin administration were stained for lineage markers and α-SMA and the proportion of α-SMA^+ cells was evaluated by flow cytometry. **E** and **F**: Lungs from Col1a2-GFP mice at 14 days after saline (**E**) or bleomycin (**E** and **F**) administration were stained with antibodies against PI and α-SMA (**E**) or PI and collagen type I (**F**). **Boxed** regions in the Merge column correspond to images in the Enlarge column. Original magnification, ×400. Data are expressed as means ± SEM (**D**) or as both means ± SEM and individual data points (**C**). $n = 4$ or 6 (**C**); $n = 3$ or 4 (**D**). $^*P < 0.05$, $^{**}P < 0.01$. Scale bar = 500 μm.

(Figure 4B). In contrast, the proportion of epithelial cells that were apoptotic dramatically increased after bleomycin treatment, from 1.3 ± 0.2% in untreated mice to 6.0 ± 0.3% on day 14 after bleomycin treatment (Figure 4B). This result highlights the severe injury sustained by the lung epithelium during bleomycin-induced fibrosis. Unlike endothelial and epithelial cells, in GFP$^+$ fibroblasts the apoptosis peaked at day 7, although the proportion of apoptotic cells observed on day 14 remained elevated above those seen at day 0 (Figure 4B).

We also examined the apoptosis of tissue cells using ROSA-CAG-SCAT3.1 knockin mice (SCAT3.1 mice), in which apoptotic cells are detected with fluorescent fusion protein.[17,30,31] In these mice, apoptotic cells form a population with a reduced fluorescence resonance energy transfer (FRET) signal and a slightly elevated ECFP signal, compared with nonapoptotic cells (Supplemental Figure S4). The kinetics of apoptosis obtained with SCAT3.1 mice were similar to those obtained with anti-cleaved caspase 3 antibody (Supplemental Figure S5). These results demonstrate the different sensitivities of tissue cells to apoptosis during the lung remodeling caused by bleomycin.

We next used BrdU to investigate the proliferation of lung tissue cells during bleomycin-induced fibrosis. At 24 hours after bleomycin-treated Col1a2-GFP mice were injected intraperitoneally with BrdU, their lungs were harvested and the number of BrdU$^+$ cells present was counted by flow cytometry (Figure 4C). Uptake of BrdU by endothelial cells peaked at day 7 and then gradually decreased (Figure 4D). Uptake by epithelial cells similarly peaked at day 7, but was sustained at similar levels at days 14 and 21 (Figure 4D). GFP$^+$ fibroblasts also had the greatest BrdU incorporation at 7 days after bleomycin administration, followed by a steady decrease across days 14 and 21 (Figure 4D), a pattern similar

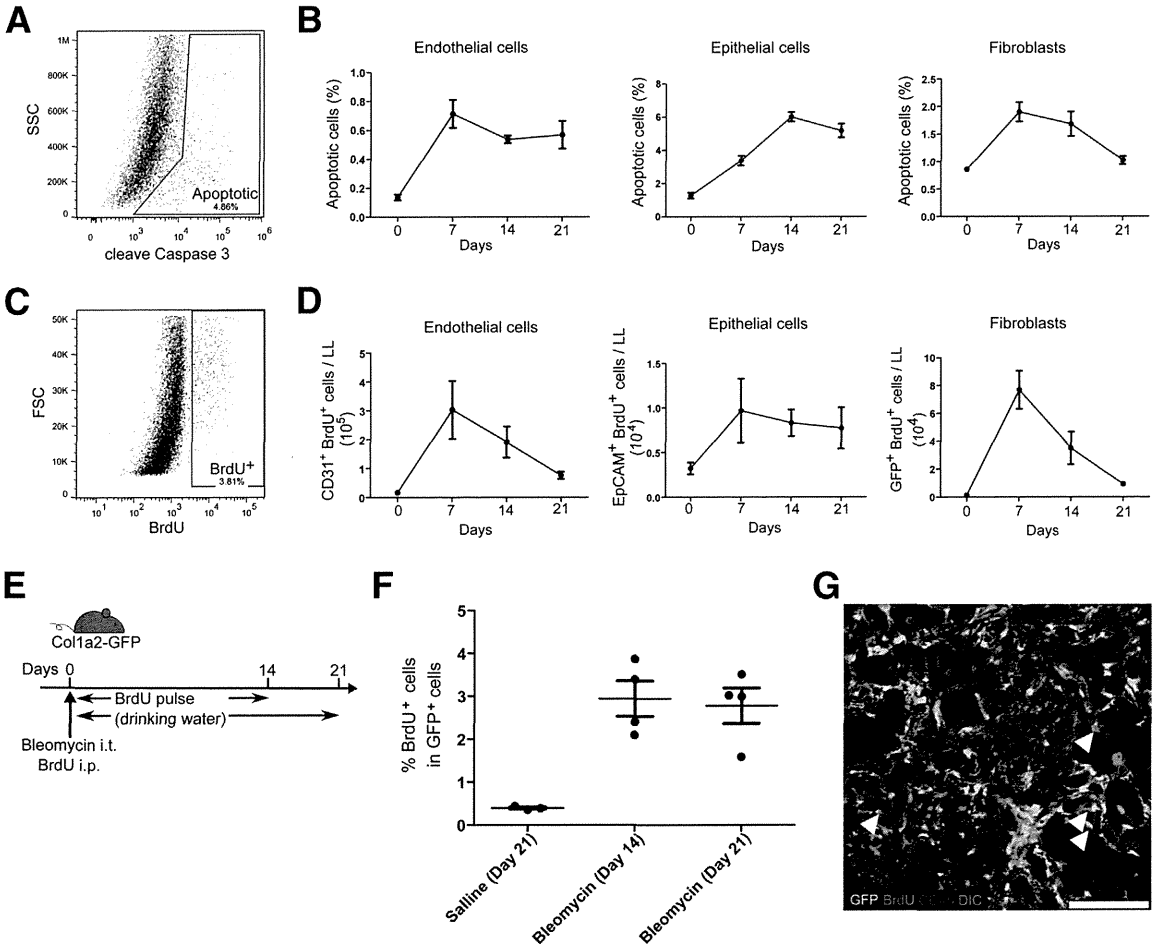

Figure 4 Proliferation and apoptosis of fibroblasts in bleomycin-induced pulmonary fibrosis. **A:** Identification of apoptotic cells by flow cytometry with anti-cleaved caspase 3 antibody. **B:** The proportion of apoptotic cells in different lung cell populations from Col1a2-GFP mice at 0, 7, 14, and 21 days after bleomycin administration was analyzed by flow cytometry after staining for CD31 (endothelial cells), EpCAM (epithelial cells), and CD45 (leukocytes). **C:** Identification of BrdU$^+$ cells by flow cytometry. **D:** Col1a2-GFP mice were pulsed with BrdU for 24 hours before analysis at 0, 7, 14, or 21 days after bleomycin administration. Lung cells were stained for BrdU and CD31, EpCAM, and CD45 and BrdU$^+$ cell numbers were quantitated. **E:** Experimental design for long-term BrdU pulse experiments. **F:** After long-term BrdU pulse, lung cells were stained for BrdU and analyzed for the proportion of BrdU$^+$ cells among GFP$^+$ cells. **G:** Representative lung section from Col1a2-GFP mice at 14 days after bleomycin administration and long-term BrdU pulse, with staining for GFP (green), BrdU (red), and CD45 (blue). BrdU$^+$ GFP$^+$ cells are indicated by **arrowheads**. DIC is also shown (gray). Data are expressed as means ± SEM (**B** and **F**) or as both means ± SEM and individual data points (**D**). n = 3 or 4. Scale bar = 100 μm.

to that observed for apoptotic Lin^- cells (Figure 4B). Similar experiments using fluorescent ubiquitination-based cell cycle indicator (Fucci) mice (FucciG1-#639 and FucciS/G2/M-#474 double-transgenic mice), which enable quantification of proliferating cells independent of pulse time,[32] yielded results consistent with those obtained from BrdU-uptake experiments (Supplemental Figure S6).

To examine whether GFP^+ fibroblast clusters are dependent on cell proliferation, we treated Col1a2-GFP mice with a long-term BrdU pulse after bleomycin treatment (Figure 4E). In this experiment, approximately 30% of $CD45^+$ leukocytes in the lungs were $BrdU^+$ at day 14 or 21 after bleomycin treatment (Supplemental Figure S7). More than 10% of endothelial and epithelial cells were $BrdU^+$ at day 21 after bleomycin treatment (Supplemental Figure S7). In contrast, only 3% of GFP^+ cells in bleomycin-treated mice (day 14 and 21) were $BrdU^+$ (Figure 4F). Immunofluorescence staining of lung sections from bleomycin-treated mice (day 14) revealed BrdU staining among $CD45^+$ leukocytes and other stromal cells, which might have included endothelial and epithelial cells (Figure 4G and Supplemental Figure S7). However, only a small portion of GFP^+ cells were $BrdU^+$ (Figure 4G), and most of the GFP^+ cells in fibrotic clusters were $BrdU^-$, suggesting that the clusters do not form through proliferation alone.

In summary, bleomycin treatment induced both apoptosis and proliferation of lung tissue cells. Although proliferative GFP^+ fibroblasts were detected, particularly in the early phase of fibrosis, the concurrent induction of apoptosis kept the overall number of GFP^+ fibroblasts constant, and for the most part the GFP^+ fibroblast clusters were not formed only by proliferation.

The Contribution of Bone Marrow-Derived Cells to the Lung GFP^+ Fibroblast Population

Several studies have reported that $CD45^+$ collagen type I-positive circulating mesenchymal cells (so-called fibrocytes) contribute to fibrogenesis after bleomycin-induced lung injury.[33,34] However, we detected almost no GFP^+ cells in the peripheral blood cells, most of which were $CD45^+$, of saline- or bleomycin-treated Col1a2-GFP mice at day 14 after treatment (Figure 5A). To investigate the extent to which lung GFP^+ fibroblasts were supplied from the bone marrow via the circulation, we generated parabiotic pairs composed of Col1a2-GFP ($CD45.2^+$) and congenic wild-type (WT; $CD45.1^+$) mice (Figure 5B). At 6 weeks after surgery, we treated mice with bleomycin or saline. Lungs were then harvested at day 21 after bleomycin treatment for analysis by flow cytometry. Chimerism of 40% to 60% (B-cell congenic markers) was observed, demonstrating that circulating blood was shared in the parabiotic mice (Figure 5C). However, in WT lungs only a very small proportion (<0.5%) of Lin^- cells were GFP^+ after treatment with either saline or bleomycin (Figure 5D). Similarly, fluorescent microscopy analysis of lung sections at 21 days after bleomycin treatment did not detect any GFP^+ fibroblasts in WT lungs, in stark contrast to the GFP^+ fibroblasts that were prominent in fibrotic regions of Col1a2-GFP lungs (Figure 5E). These results suggest that the GFP^+ fibroblasts in fibrotic regions in the lungs are not supplied from the bone marrow or the circulation during fibrosis. Instead, resident cells in the lungs, probably resident fibroblasts, are the likely progenitors of the activated fibroblasts that form fibrotic regions.

Gene Expression Analysis of GFP^+ Fibroblasts

To further investigate phenotypic changes in GFP^+ fibroblasts, we generated a whole-genome gene expression profile for these cells. We used next-generation sequencing to perform SAGE analysis on GFP^+ lung fibroblasts sorted by fluorescence-activated cell sorting at 14 days after saline or bleomycin treatment. The purity of GFP^+ cells after sorting was 94.5% and 98.0% for saline and bleomycin treatment, respectively. We identified 2,973,937 SAGE tags (1,080,798 tags from saline-treated GFP^+ fibroblasts and 1,893,139 tags from bleomycin-treated GFP^+ fibroblasts), representing 13,894 distinct transcripts. The number of tag sequences from bleomycin-treated GFP^+ fibroblasts was normalized to that of saline-treated GFP^+ fibroblasts before gene expression was compared between the two libraries. There were 213 genes with a greater than threefold difference between the saline and bleomycin groups. The 40 transcripts that increased the most after bleomycin treatment, compared with control, are listed in Table 1. The 40 genes that were most down-regulated are listed in Supplemental Table S1. The most highly up-regulated transcript (213-fold) was secreted phosphoprotein 1 (*Spp1*). To confirm the SAGE results, qPCR was performed for representative transcripts. There was good correlation between the results of the SAGE and qPCR analyses (Supplemental Figure S8).

Some of the 40 most up-regulated genes that were induced by bleomycin treatment have already been identified as important in fibrosis. *Spp1* is known to be up-regulated in idiopathic pulmonary fibrosis patients, as well as in the bleomycin-induced lung fibrosis model in mice.[35,36] Cytokine receptor-like factor 1 (*Crlf1*) expressed by epithelial cells was recently reported to have antifibrotic actions.[37] The present data, however, suggest that fibroblasts also express *Crlf1*. The expression of S100a4, a fibroblast marker, was low in saline-treated mice but dramatically up-regulated in bleomycin-treated mice. Gelsolin (*Gsn*), which is involved in the rearrangement of cytoskeletal structure and is necessary for the development of pulmonary fibrosis,[38] showed a remarkable decrease of tag number, from 19,346 to 2548 (Supplemental Table S1). Interestingly, expression of the latent transforming growth factor β binding protein 4 gene (*Ltbp4*) decreased markedly at day 14 after bleomycin treatment (Supplemental Table S1). Ltbp4 regulates TGF-β1 bioavailability in pulmonary fibrosis.[39] Despite these insights into how changes in fibroblast gene expression can influence fibrogenesis, the significance of changes in the expression of many other genes remains elusive.

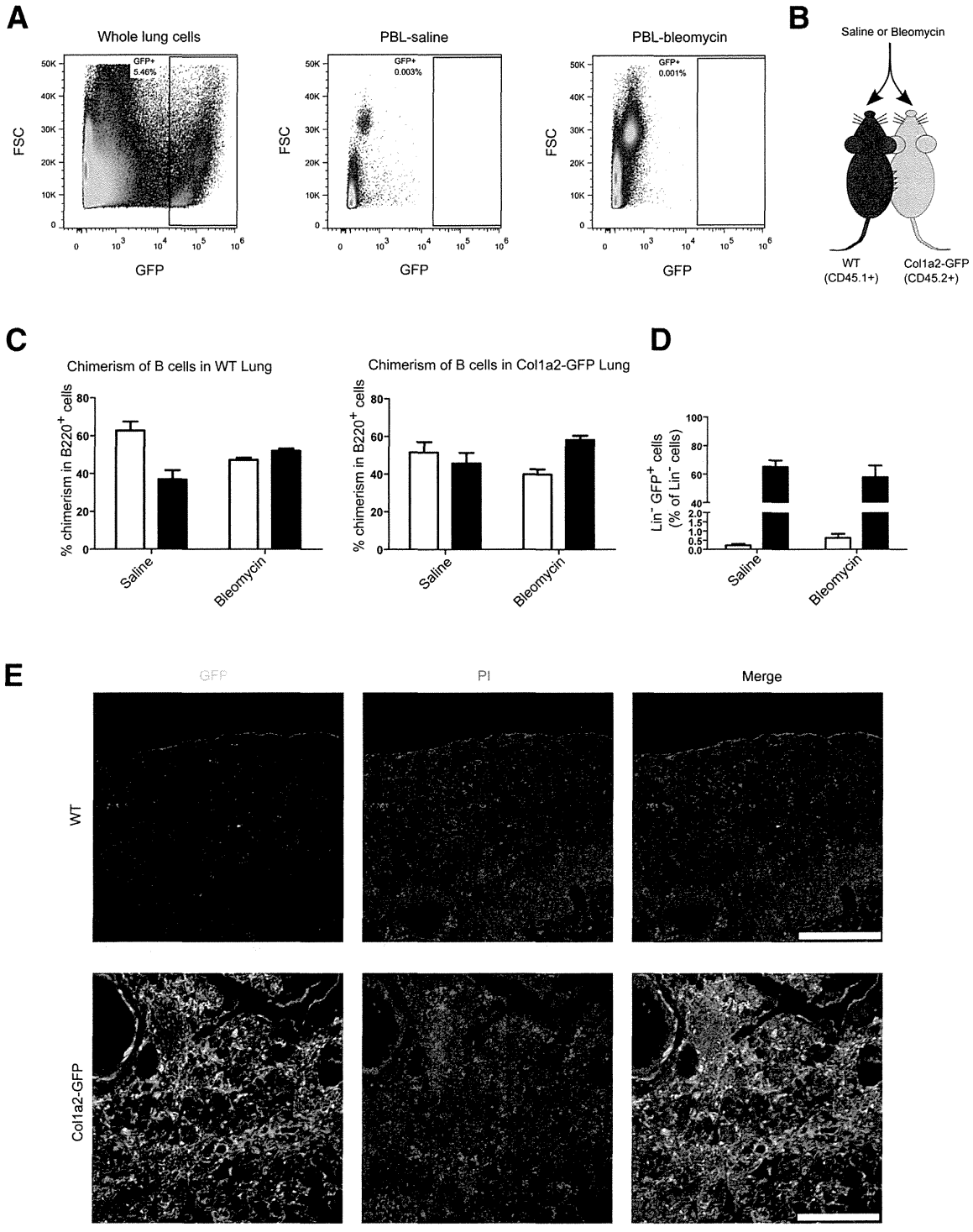

Figure 5 The contribution of bone marrow-derived cells to the lung GFP$^+$ fibroblast population. **A:** Whole-lung cells (saline treatment) and peripheral blood cells (saline or bleomycin treatment) were analyzed by flow cytometry at 14 days after treatment. Red plots are dense area, and blue plots are sparse area. **B:** Parabiotic pairs of WT (CD45.1$^+$) mice and Col1a2-GFP mice (CD45.2$^+$) were intratracheally instilled with bleomycin or saline. Each parabiotic pair received the same treatment. **C:** Chimerism of B cells (B220$^+$ cells) in the lungs of WT (white bars) or Col1a2-GFP (black bars) mice was determined from CD45.1 and CD45.2 expression. **D:** The proportion of GFP$^+$ cells in WT (white bars) and Col1a2-GFP (black bars) lungs was measured by flow cytometry. **E:** Representative lung sections of parabiotic WT and Col1a2-GFP mice stained for GFP and PI and imaged by confocal fluorescence microscopy. Data are expressed as means ± SEM (**C** and **D**). Scale bar = 250 μm. PBL, peripheral blood.

Previous studies have demonstrated roles for TGF-β, EGF, and IL-1β in pulmonary fibrosis.[5,40,41] By analyzing the gene expression profiles of fibroblasts with IPA software, we confirmed that these molecules worked directly as upstream gene regulators in fibroblasts (Supplemental Table S2). We also categorized up-regulated genes by molecular function, such as cytokine, chemotaxis, cell adhesion, and DNA binding (Supplemental Tables S3, S4, S5, and S6)

Table 1 The 40 Most up-Regulated Genes in GFP$^+$ Fibroblasts at 14 Days after Bleomycin Treatment

Symbol	Tags, no.		Fold change
	Saline	Bleomycin	
Spp1	57	12,155	213.2
Crlf1	1	212	212.0
Chl1	1	157	157.0
Cthrc1	1	97	97.0
Ereg	7	449	64.1
Anxa8	2	108	54.0
Lrg1	2	104	52.0
Hp	28	1,077	38.5
9930013L23Rik	4	103	25.8
Gjb3	4	98	24.5
C1qtnf6	13	298	22.9
Sdc1	6	136	22.7
Areg	3	66	22.0
Tnc	40	824	20.6
S100a4	116	2,060	17.8
Fst	36	568	15.8
Ildr2	6	86	14.3
Mcm6	6	74	12.3
Hspb7	9	106	11.8
Timp1	163	1,883	11.6
Slc7a2	8	88	11.0
Sfrp1	165	1,702	10.3
Fkbp5	10	95	9.5
Serpina3m	18	164	9.1
Rnf149	21	191	9.1
Fn1	1018	8,890	8.7
Chst11	10	87	8.7
Il11	8	66	8.3
*Nrep**	48	395	8.2
Cd109	16	118	7.4
1110038B12Rik	15	107	7.1
Slpi	23	164	7.1
Rgs16	25	176	7.0
Cyp26b1	11	75	6.8
Saa3	219	1,474	6.7
Nek6	12	78	6.5
Inhba	14	90	6.4
Col12a1	30	189	6.3
Col7a1	19	118	6.2
Wisp1	30	180	6.0

*Alias *D0H4S114*.

To assess the functional significance of changes in the gene expression profile of GFP$^+$ fibroblasts after bleomycin treatment, we used DAVID software to analyze which GO terms were enriched among genes that were up-regulated greater than threefold (Table 2).[21] Many of the up-regulated genes related to the ECM, suggesting that after bleomycin treatment the activated GFP$^+$ fibroblasts were involved in construction of ECM networks at fibrotic lesions. Genes related to the binding of extracellular components, such as glycosaminoglycan, were also up-regulated. We also used IPA software to quantify the specific changes in biological function associated with changes in gene expression in activated GFP$^+$ fibroblasts (Table 3). The IPA analysis yields an activation z-score that indicates the extent to which biological function is increased (positive values) or decreased (negative values). Genes that promote cell proliferation were up-regulated in activated GFP$^+$ fibroblasts, whereas functions linked to cell death, such as apoptosis and necrosis, had negative activation z-scores. These results indicate that activated GFP$^+$ fibroblasts are more resistant to cell death. Functions related to cell migration (including cell movement, invasion, and chemotaxis) were increased. Overall, these results mirror the assumed roles of fibroblasts in fibrogenesis; activated fibroblasts migrate to damaged sites and generate fibrotic legions by secreting ECM components. These data also support a central role for GFP$^+$ fibroblasts in bleomycin-induced fibrogenesis.

Identification of OPN as an Early Activation Marker of Lung Fibroblasts in Bleomycin-Induced Fibrosis

Because the OPN gene *Spp1* had both the highest fold change and the high read tag number in bleomycin-treated GFP$^+$ fibroblasts, we examined the possibility that OPN might serve as an activation marker for lung fibroblasts. Although T cells and macrophages are well-known sources of OPN, tissue cells may be important alternative sources of this protein.[42] We used qPCR to confirm *Spp1* expression levels in mRNA collected from sorted GFP$^+$ fibroblasts. *Spp1* mRNA levels were approximately 500 times higher in bleomycin-treated fibroblasts than in saline-treated fibroblasts (Figure 6A). To confirm protein expression, we cultured lung fibroblasts with BFA and stained them with an antibody against OPN before analysis by flow cytometry (Figure 6B). Of the Lin$^-$ bleomycin-treated GFP$^+$ fibroblasts, 9.0 $\pm$ 1.1% were OPN$^+$, compared with only 0.37 $\pm$ 0.07% of saline-treated GFP$^+$ fibroblasts (Figure 6C).

Table 2 Gene Ontology (GO) Terms That Were Enriched Amongst Genes That Were up-Regulated Greater than Threefold in GFP$^+$ Fibroblasts at 14 Days after Bleomycin Treatment

GO term	Genes, no.	*P* value
Extracellular region	40	2.58×10^{-14}
Extracellular region part	25	4.17×10^{-11}
Extracellular matrix part	11	3.04×10^{-10}
Proteinaceous extracellular matrix	16	5.03×10^{-10}
Extracellular matrix	16	8.70×10^{-10}
Collagen	5	5.60×10^{-06}
Cell adhesion	14	4.81×10^{-05}
Biological adhesion	14	4.90×10^{-05}
Glycosaminoglycan binding	7	7.71×10^{-05}
Basement membrane	6	1.01×10^{-04}
Pattern binding	7	1.46×10^{-04}
Polysaccharide binding	7	1.46×10^{-04}
Heparin binding	6	1.67×10^{-04}
Growth factor activity	7	2.48×10^{-04}
Extracellular structure organization	7	3.59×10^{-04}
Extracellular matrix organization	6	4.44×10^{-04}